https://doi.org/10.5194/egusphere-2026-6579
Preprint. Discussion started: 9 November 2026
© Author(s) 2026. CC BY 4.0 License.

# Precipitation–soil-moisture dominance and hydrograph signatures of floods: large-sample evidence across diverse catchments

Yifat Kimchi[1], Efrat Morin[1]

[1]The Fredy and Nadine Herrmann Institute of Earth Sciences, the Hebrew University of Jerusalem, Jerusalem, 9190401, Israel

*Correspondence to*: Yifat Kimchi (yifat.kimchi@mail.huji.ac.il) and Efrat Morin (efrat.morin@mail.huji.ac.il)

**Abstract.** Precipitation and antecedent soil moisture jointly shape floods, but how their relative influence varies among individual floods, and how that variation is expressed in flood behavior, remains poorly resolved. We developed an event-based framework to quantify their relative predictive contributions to annual-maximum floods across diverse non-snow catchments. A catchment-shared Light Gradient Boosting Machine (LightGBM) model predicted daily streamflow percentile from 3-day accumulated precipitation ($t-2$ to $t$) and soil moisture in four layers at $t-3$. Shapley additive explanations (SHAP) decomposed annual-maximum predictions into model-attributed contributions, combined into a continuous event-level dominance index ($D$) ranging from −1 (soil-moisture dominance) to +1 (precipitation dominance). Applied to GRDC-Caravan, the model reached a median catchment-wise Nash–Sutcliffe efficiency (NSE) of 0.594 in percentile space. After quality control, we analyzed 32,930 annual-maximum events from 1,209 catchments worldwide. Precipitation was the strongest single predictor in 56.5 % of events, yet the four soil-moisture layers' combined net contribution exceeded it in 71.4 % (66.6–87.8 % across tested predictor configurations). High streamflow percentiles arose from either moderate precipitation over very wet soils or very high precipitation over drier soils; the highest percentiles combined high precipitation with wet antecedent conditions. Increasing precipitation dominance was moderately associated with faster pre-peak rises ($\rho$ = 0.466) and weakly with higher peaks ($\rho$ = 0.191), faster recessions ($\rho$ = 0.182), and precipitation closer to the peak ($\rho$ = 0.156). Within catchments, the rising-limb association persisted ($\rho$ = 0.417), while the peak-magnitude association was much weaker ($\rho$ = 0.092). Precipitation-dominated floods began from drier soils and showed rapid shallow-layer wetting, while deeper layers stayed drier throughout the event window. Catchment-mean dominance shifted toward precipitation in steeper (partial $\rho$ = 0.286) and smaller (partial $\rho$ = −0.185) catchments, with weaker differentiation among climate zones. Yet 94.2 % of the 1,154 catchments with at least 10 events contained floods on both sides of the index, and within-catchment differences accounted for 73.1 % of the variation in $D$. Flood behavior therefore reflects an event-specific balance between forcing and antecedent storage rather than a fixed catchment property.

## 1 Introduction

Flood generation results from the interaction between meteorological forcing and antecedent catchment state (e.g., Ivancic and Shaw, 2015; Sharma et al., 2018; Wasko et al., 2021; Wasko and Nathan, 2019). In non-snow catchments, antecedent state is

https://doi.org/10.5194/egusphere-2026-6579
Preprint. Discussion started: 9 November 2026
© Author(s) 2026. CC BY 4.0 License.

mainly expressed through soil moisture (Berghuijs et al., 2016; Collins, 2019; Wasko et al., 2021). Catchment characteristics shape flood sensitivity to precipitation and antecedent wetness, but these controls' relative influence varies among floods within and across catchments (Brunner and Dougherty, 2022; Jiang et al., 2022b, 2024a; Merz and Blöschl, 2003; Stein et al., 2020, 2021; Tarasova et al., 2019, 2020). This event-to-event variability suggests that individual floods can be characterized by the relative dominance of precipitation and antecedent soil moisture. This characterization enables an examination of how these controls shape flood magnitude and hydrograph dynamics. This requires event-specific information on forcing and antecedent wetness rather than long-term seasonal or climatological indicators. Large-sample analyses can then determine whether these controls are associated with consistent patterns across hydroclimatic and physiographic settings (Addor et al., 2020). Although the interaction between precipitation and soil moisture is well established, their relative importance for individual floods, the conditions favoring each control, and how this dominance is reflected in flood magnitude and hydrograph dynamics remain less understood.

Large-sample studies have advanced understanding of flood-generating processes by identifying their hydroclimatic controls. Because our analysis covers non-snow catchments, we focus on how large-sample studies distinguish precipitation forcing from antecedent soil-moisture control. Existing studies broadly follow three methodological strategies. Seasonality-based approaches compare the long-term timing and variability of annual floods with those of hypothesized controllers. Across the contiguous United States (CONUS) and Europe, Berghuijs et al. (2016, 2019) inferred dominant or relative catchment-level controls by comparing annual-flood seasonality with precipitation, precipitation-excess estimates, and snowmelt. These methods rely on aggregated seasonal patterns and cannot resolve individual flood controls. A second strategy classifies individual floods using predefined rules and thresholds (e.g., Merz and Blöschl, 2003; Stein et al., 2020). Stein et al. (2020) combined precipitation with modeled soil-moisture and snowmelt indicators to assign annual maxima worldwide to manually predefined processes. Brunner and Dougherty (2022) classified storm types and threshold-defined soil-moisture and snowmelt conditions across CONUS and compared their combinations between local and regional floods. Such approaches retain event-level information but depend on the selected definitions, decision structure, and thresholds.

A third strategy uses explainable machine learning to interpret rainfall–runoff models through feature-contribution patterns. Jiang et al. (2022a, b) used catchment-specific recurrent models with precipitation and temperature sequences across CONUS and Europe to classify flood peaks and examine temporal changes in their occurrence. Shen and Chui (2023) used tree ensembles with rainfall, temperature, estimated precipitation-excess, snowmelt, and effective precipitation to quantify their relative predictive contributions to flood peaks across CONUS. Xu et al. (2024) used catchment-specific deep-learning models with precipitation, soil-water layers, snow depth, and other inputs across the United States to identify dominant controls and analyze antecedent lags, interactions, and temporal changes. Jiang et al. (2024a) used tree ensembles and explanatory interaction values worldwide to quantify individual and compounding contributions of rainfall, temperature, soil moisture, and snowpack, showing that multi-driver floods, particularly rainfall–soil-moisture combinations, are widespread. These approaches capture nonlinear relationships and support event-scale analysis, but their feature attributions represent modeled predictive associations rather than direct causal contributions of hydrological processes. Outside these strategies, Ran et al.

https://doi.org/10.5194/egusphere-2026-6579
Preprint. Discussion started: 9 November 2026
© Author(s) 2026. CC BY 4.0 License.

(2022) used catchment-level ratios to compare modeled antecedent soil-water storage and flood-day precipitation in China's middle–lower Yangtze catchment, averaging conditions across annual floods.

These studies characterize antecedent wetness using indicators that reflect soil-moisture conditions more or less directly, from precipitation-excess estimates, modeled bulk storage, threshold-defined classes, and historical precipitation proxies to direct soil-moisture inputs. These representations distinguish stronger wetness control (e.g., rainfall on near-saturated soil) from stronger precipitation control (e.g., short, intense rainfall), while allowing combined mechanisms. Nevertheless, these studies do not fully address our target setting. Many studies categorize floods or catchments into predefined mechanisms; even studies calculating event-based contributions often summarize results at catchment level, obscuring within-catchment variability. Soil moisture is commonly represented through thresholds or as a bulk state, leaving its event-specific and depth-dependent contributions insufficiently resolved. Although global studies exist, detailed evidence remains concentrated in North America and Europe. Links between inferred controls and streamflow dynamics, including flood magnitude, hydrograph shape, and timing, also remain weak. An interpretable, event-scale, multi-continental framework is therefore needed to decompose flood-peak predictions into near-event precipitation and multi-depth antecedent soil moisture contributions, quantify their continuous balance, and relate it to flood behavior and catchment characteristics.

Machine-learning models offer a promising approach to address these gaps by capturing nonlinear relationships between meteorological forcing, catchment state, and streamflow across large samples (Slater et al., 2025). Long short-term memory (LSTM) networks show strong predictive skill and realistic system behavior (Kratzert et al., 2018, 2019a; Shen, 2018), but encode antecedent information through sequential inputs and recurrent memory, complicating direct attribution to explicitly separated near-event precipitation and antecedent-state predictors. Tree ensemble models instead operate on an explicitly defined predictor set, facilitating attribution of individual predictions to precipitation and antecedent soil-moisture variables. Feature-attribution techniques such as Shapley additive explanations (SHAP; Lundberg and Lee, 2017) further decompose model predictions into contributions from individual inputs. However, most studies fit catchment-specific models, whose explanations originate from different fitted functions, making attribution patterns less directly comparable across catchments. Training one model across catchments provides a common predictive and interpretive framework for learning shared relationships across climatic and physiographic settings.

In this study, we present an event-based framework combining explainable machine learning with large-sample hydrological data to quantify the relative predictive contributions of precipitation and antecedent soil moisture to annual-maximum floods across diverse non-snow catchments. We call the relative balance of these model-attributed predictive contributions predictive dominance, or simply dominance. This term describes attribution within the fitted model without implying causal control by the corresponding hydrological processes. Using daily streamflow, precipitation, and multi-depth soil-moisture data from GRDC-Caravan (Färber et al., 2025a), a multi-continental extension of Caravan based on streamflow records from the Global Runoff Data Centre (GRDC), we train a catchment-shared Light Gradient Boosting Machine (LightGBM; Ke et al., 2017) tree ensemble model and apply SHAP to decompose annual-maximum predictions into contributions from near-event precipitation and antecedent wetness. We combine these contributions into a continuous predictive dominance index ($D$) ranging from soil-

https://doi.org/10.5194/egusphere-2026-6579
Preprint. Discussion started: 9 November 2026
© Author(s) 2026. CC BY 4.0 License.

moisture to precipitation dominance, retaining event-to-event variability rather than assigning floods or catchments to fixed classes. Restricting predictors to key hydrological controls and immediate pre-event conditions gives the framework a consistent, interpretable representation of forcing and antecedent storage and allows extension to additional catchments with comparable data. We examine how flood magnitude, hydrograph dynamics, precipitation timing, and individual soil-moisture layer dynamics vary along the dominance gradient, and how catchment-level dominance relates to climatic and physiographic attributes. By linking continuous dominance to flood behavior, catchment properties, and the vertical structure of antecedent wetness, the study advances event-based understanding of precipitation–soil-moisture controls on floods across diverse catchments.

## 2 Data and methodology

### 2.1 Data

We used GRDC-Caravan (Färber et al., 2025a, b; https://zenodo.org/records/15349031, last accessed: 28 May 2025), which integrates meteorological forcing, catchment attributes, and streamflow data within Caravan's standardized global framework (Kratzert et al., 2023). The dataset includes 5,356 catchments worldwide (Fig. 1), with daily observed streamflow, catchment metadata, and boundaries from GRDC; catchment attributes from HydroATLAS (Linke et al., 2019) and catchment-average daily meteorological forcing and land-surface state variables from ERA5-Land reanalysis (Muñoz-Sabater et al., 2021).

We restricted the analysis to catchments with at least five valid hydrological years of streamflow observations between 1 September 1979 and 31 August 2022. Hydrological years ran from 1 September to 31 August and were labeled by their ending year (1980–2022). We excluded years with less than 75 % streamflow-data coverage (< 274 days); the five-year requirement ensured sufficient training samples per catchment. The study period began in 1979 to align with the satellite era, when assimilating global satellite observations improved reanalysis quality (Hersbach et al., 2020) and ended in hydrological year 2022, the dataset's last complete year. To exclude snow-related storage and phase-change processes, we retained only catchments with a GRDC-Caravan snow fraction of zero, defined as the fraction of mean monthly precipitation occurring in months with mean monthly 2 m air temperature below 0 °C (Knoben et al., 2018; Kratzert et al., 2023). We restricted catchment areas to 100–5,000 km² to reduce scale mismatches with the approximately 81 km² ERA5-Land grid cells and exclude very large catchments whose slower hydrological responses and catchment-averaged inputs may obscure event-scale dynamics. These filters retained 1,374 catchments for model training and evaluation.

For each catchment, we extracted daily streamflow, precipitation, and volumetric soil moisture for the four ERA5-Land soil layers (0–7, 7–28, 28–100, and 100–289 cm). Precipitation and soil moisture in the Caravan datasets are derived from ERA5-Land, which provides globally consistent meteorological forcing and land-surface states at ~9 km spatial resolution (Muñoz-Sabater et al., 2021). ERA5-Land precipitation is downscaled from ERA5 atmospheric forcing (~31 km), whereas soil moisture is simulated by the Carbon Hydrology Tiled ECMWF Scheme for Surface Exchanges over Land (CHTESSEL), which represents the land water and energy balances (Hersbach et al., 2020; Muñoz-Sabater et al., 2021). ERA5-Land thus provides

https://doi.org/10.5194/egusphere-2026-6579
Preprint. Discussion started: 9 November 2026
© Author(s) 2026. CC BY 4.0 License.

long-term, spatially complete, and internally consistent precipitation and multi-depth soil-moisture estimates over the same spatial and temporal support. Satellite soil-moisture products provide valuable observational constraints, but shorter records, limited sensitivity to deeper soil layers, and incomplete spatial or temporal coverage limit their suitability as primary data for this multi-continental event-based analysis. ERA5-Land precipitation and soil moisture have been widely used and evaluated in hydrological and land-surface applications (e.g., Bandhauer et al., 2022; Beck et al., 2019, 2021; Jiang et al., 2021; Su et al., 2025; Tang et al., 2020; Xu et al., 2022). To further assess its suitability, we evaluated ERA5-Land soil moisture against independent in situ observations from the International Soil Moisture Network (ISMN; Dorigo et al., 2011, 2021). The evaluation (Supplement S1) indicated predominantly systematic ERA5-Land soil-moisture biases, largely consisting of shifts and rescaling that preserve the temporal ordering of wet and dry conditions. Such monotonic biases should have limited influence on tree-based models, which depend primarily on predictor ordering rather than absolute magnitudes. Accordingly, we retained the original ERA5-Land soil-moisture data for the main analysis.

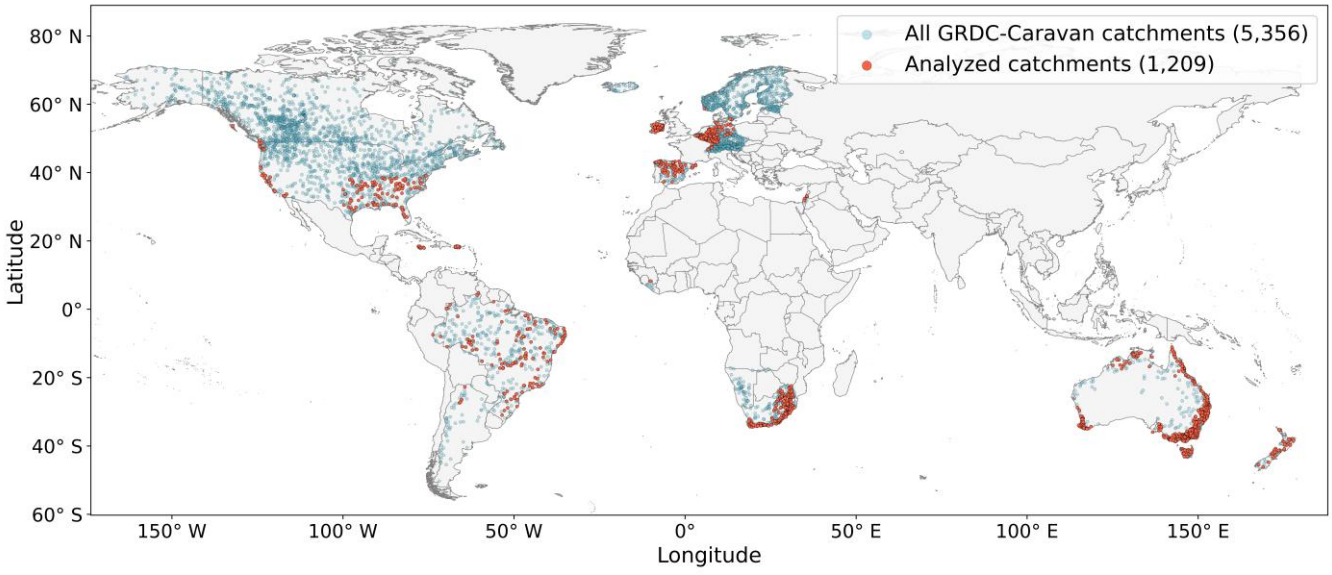



**Figure 1:** Geographic distribution of GRDC-Caravan catchments. Blue points show all 5,356 GRDC catchments in GRDC-Caravan; red points show the 1,209 retained for SHAP-based interpretation after filtering for catchment size, snow influence, data availability, event integrity, and model performance (Sect. 2.4).

### 2.2 Model target and predictor construction

To compare catchments with diverse characteristics and flow regimes, we transformed target and predictor variables into catchment-specific percentiles between 0 and 1, using each catchment's retained record. Positive observations were assigned ranks, averaged for ties, and these ranks were divided by the number of positive observations; zeros and missing values were preserved. The target variable was the streamflow percentile on day $t$. Predictors comprised 3-day accumulated precipitation over $t-2$ to $t$ and soil moisture from the four layers on day $t-3$. This configuration captures short-term precipitation forcing and antecedent wetness relevant to event-scale flood analysis while temporally separating the soil-moisture state from the

https://doi.org/10.5194/egusphere-2026-6579
Preprint. Discussion started: 9 November 2026
© Author(s) 2026. CC BY 4.0 License.

subsequent precipitation window. Empirical catchment lag-time estimates and tests of alternative predictor configurations guided predictor timing (Supplement S2). The selected setup provided a practical compromise between physical consistency, event-scale interpretation, sample size, and predictive performance.

### 2.3 Modeling framework

Although interpretation focuses on annual-maximum flood events, we trained the model on all eligible daily observations. Training on daily observations enabled continuous streamflow predictions around each annual maximum, supporting analysis of hydrograph dynamics rather than peak magnitude alone. It also broadened the hydrological conditions represented and substantially increased the training sample, supporting robust model fitting across diverse catchments.

For this multi-continental study, we used machine learning to learn and compare relationships across catchments within a single, consistent, scalable model (Kratzert et al., 2024). We trained a catchment-shared Light Gradient Boosting Machine (LightGBM; Ke et al., 2017) model to predict daily streamflow percentiles from the predictor variables. LightGBM is a gradient-boosted decision-tree ensemble well-suited to large datasets and nonlinear predictor interactions. Its histogram-based split finding and leaf-wise tree growth enable efficient training while retaining predictive flexibility (Ke et al., 2017). Among the tree-based models tested in preliminary experiments, LightGBM offered the best combination of predictive skill and computational efficiency, so we selected it over random forest and XGBoost.

We tuned hyperparameters on the training data using grid search (Supplement S3, Table S3). The final configuration used a learning rate of 0.1, a maximum tree depth of 12, 511 leaves per tree, a minimum of 500 samples per leaf, L2 regularization ($\lambda$ = 1.0), a bagging fraction of 0.8, and a maximum of 2000 boosting iterations. This limit allowed training until predictive performance plateaued, with early stopping selecting the effective number of trees. These settings balanced model flexibility and regularization while capturing nonlinear interactions.

We performed model training, evaluation, and interpretation using repeated five-fold blocked cross-validation on daily streamflow samples. Each block kept all daily samples from one catchment–hydrological-year combination in the same fold. In each repetition, four folds formed the training pool and the fifth served as the held-out validation fold. We repeated the five-fold procedure five times with different random block assignments, yielding 25 fitted models and corresponding validation sets. This repetition reduced sensitivity to any single data partition (Jiang et al., 2024b).

For each model fit, we split the training pool while preserving catchment–hydrological year blocks, using approximately 80 % for model fitting and 20 % for early stopping to determine the number of boosting iterations. Training stopped when the root mean squared error (RMSE) failed to improve by at least $10^{-3}$ for 300 consecutive iterations, resulting in approximately 600–950 trees per model, below the 2000-tree limit. The models were not subsequently refitted on the full training pool; consequently, each model was trained on approximately 64 % of all daily samples. The held-out validation fold served exclusively for prediction and performance evaluation, excluding it from model fitting and early stopping.

Separating model fitting, early stopping, and final evaluation limited information leakage, optimistic performance estimates, and overfitting. Each day received five out-of-fold predictions, one per repetition, with that day excluded from model fitting

https://doi.org/10.5194/egusphere-2026-6579
Preprint. Discussion started: 9 November 2026
© Author(s) 2026. CC BY 4.0 License.

and early stopping. We clipped each prediction to [0, 1] and averaged the five clipped predictions to obtain the final predicted daily streamflow percentile.

### 2.4 Model interpretation

The SHAP-based model interpretation focused on annual-maximum flood events, following common practice in flood-frequency analysis (e.g., Blöschl et al., 2017, 2019). We identified annual maxima from each catchment–hydrological year's observed streamflow series and retained the corresponding held-out validation predictions for analysis.

We used SHAP (Lundberg and Lee, 2017) to decompose each predicted streamflow peak into additive predictor contributions, quantifying precipitation and soil-moisture contributions. SHAP is based on Shapley values (Shapley, 1953) which quantify the average marginal contribution of a feature across all possible feature combinations. Formally, each prediction $\hat{y}_i$ is expressed as the sum of a baseline value and the contributions of all $p$ predictors:

$$\hat{y}_i = y_{base} + \sum_{j=1}^{p} \phi_{i,j} \qquad (1)$$

$y_{base}$ is the expected model output used as the SHAP baseline for each fitted model. This baseline is the mean model prediction across the observations used for model fitting and may therefore vary slightly across cross-validation models fitted on different training subsets. $\phi_{i,j}$ is the SHAP value describing the contribution of a predictor $j$ to prediction $i$. Positive SHAP values increase predictions relative to the baseline; negative values decrease them. A SHAP value's absolute magnitude reflects contribution strength; values near zero indicate negligible influence. This additive decomposition provides local explanations for individual predictions, while the global importance of a predictor $j$ can be quantified by averaging $|\phi_{i,j}|$ across all samples $i$ (Lundberg and Lee, 2017).

For tree ensembles such as LightGBM, we computed SHAP values using TreeExplainer (Lundberg et al., 2020) which efficiently calculates Shapley values from the fitted tree structure. We applied the tree-path-dependent formulation to evaluate contributions along the fitted decision paths, avoiding the assumption of independent predictor distributions. For each cross-validation model, we computed SHAP values for held-out annual-maximum events, ensuring explanations concerned predictions for samples excluded from model fitting and early stopping. Each event appeared once in validation per cross-validation repetition, yielding five SHAP contribution vectors that we averaged into a single, more stable estimate of its predictor contributions.

Because SHAP explanations are most informative when the underlying prediction is reasonably accurate, we screened the annual-maximum events after model prediction (Murdoch et al., 2019). These criteria only selected events for SHAP-based interpretation; they did not affect training, which used all eligible daily observations without identifying annual-maximum days. The post-prediction screening comprised two groups of filters. First, event-definition filters removed annual maxima unlikely to represent distinct flood peaks, including hydrological years with constant streamflow, prolonged pre-peak streamflow plateaus, low-flow annual maxima below the 60$^{th}$ streamflow percentile, and boundary events at the beginning or

https://doi.org/10.5194/egusphere-2026-6579
Preprint. Discussion started: 9 November 2026
© Author(s) 2026. CC BY 4.0 License.

end of the hydrological year that did not satisfy a local-peak condition. Second, interpretation-reliability filters removed events with missing or non-informative precipitation predictors, catchments with Nash–Sutcliffe efficiency (NSE) < 0, and events with absolute prediction error |predicted − observed| > 0.3. We selected the 0.3 event-level error threshold from the absolute prediction error distribution (Fig. 3). A stricter 0.2 threshold produced no substantial differences in dominance patterns but retained fewer events (Supplement S3, Fig. S6). We retained the 0.3 threshold to preserve a larger event sample while maintaining stable dominance patterns.

Filtering retained 32,930 annual-maximum flood events (69.8 % of the original annual maxima) for SHAP analysis from 1,209 catchments spanning diverse geographical and climatic conditions (Fig. 1). For each retained event, we extracted SHAP values for the five predictors used in the model: 3-day accumulated precipitation and soil moisture in four layers at $t-3$. The resulting event-by-predictor matrix of signed contributions underpinned the subsequent flood-control dominance analysis.

## 2.5 Dominance analysis

### 2.5.1 Dominance index

For each retained annual-maximum event, we quantified the relative predictive contributions of accumulated precipitation and antecedent soil moisture from SHAP values. The precipitation contribution $C_P$ was the absolute SHAP value of the 3-day accumulated precipitation predictor over $t-2$ to $t$. The soil-moisture contribution $C_{SM}$ was the absolute value of the sum of signed SHAP values for the four soil-moisture predictors at $t-3$. This aggregation represents the soil-moisture predictor group's net contribution, allowing opposing layer-specific effects to offset one another. We then defined a continuous event-level dominance index $D$:

$$D = \frac{C_P - C_{SM}}{C_P + C_{SM}} \qquad (2)$$

The index ranges from −1 to +1; more negative values indicate stronger soil-moisture dominance and more positive values stronger precipitation dominance. Zero indicates equal precipitation and soil-moisture contribution magnitudes. $D$ is a model-attributed predictive quantity rather than a causal partition of flood-generating processes.

The contributions differ in dimensionality: precipitation is represented by one temporally aggregated predictor, whereas soil moisture combines four layer-specific predictors. The magnitude of $D$ may therefore partly reflect predictor grouping. We retained the layer-specific representation because it preserves vertical soil-moisture variation and yielded better predictive performance than a model using mean profile soil moisture (Supplement S2, Table S2). Both representations nevertheless showed a tendency toward $D < 0$, although its magnitude differed (Supplement S2, Fig. S5). We used the continuous index $D$ as the primary measure of event-level dominance.

https://doi.org/10.5194/egusphere-2026-6579
Preprint. Discussion started: 9 November 2026
© Author(s) 2026. CC BY 4.0 License.

### 2.5.2 Event-scale dominance

We used *D* to examine flood characteristics along the transition from soil-moisture- to precipitation-dominated events. The analyses considered the joint precipitation–soil-moisture conditions, streamflow magnitude and near-peak hydrograph dynamics, relative precipitation timing, and the temporal evolution of streamflow, precipitation, and soil moisture. All streamflow characteristics and hydrographs came directly from observed daily streamflow rather than model predictions. These diagnostics used daily streamflow, precipitation, and soil-moisture catchment-specific percentiles to compare catchments with different flow regimes. Figure 2 summarizes the event-scale diagnostics and their temporal windows.

(i) **Streamflow magnitude and near-peak hydrograph slopes.** Event magnitude was represented by the peak streamflow percentile on the annual-maximum day ($t$ = 0; Fig. 2). Near-peak hydrograph dynamics were quantified using ordinary least-squares (OLS) fits to the observed streamflow-percentile series over $t - 5$ to $t$ for the pre-peak rising-limb slope and $t$ to $t + 5$ for the post-peak falling-limb slope, each comprising six daily observations (Fig. 2). For each window, the fitted relationship was:

$$\hat{q}_\tau = \alpha + \beta\tau \qquad (3)$$

$q_\tau$ is the observed daily streamflow percentile at relative day $\tau$, $\hat{q}_\tau$ is the corresponding fitted value, $\alpha$ is the fitted intercept, and $\beta$ is the fitted slope. We used $\beta$ directly for the pre-peak window and multiplied it by −1 for the post-peak window, so larger positive values indicate faster post-peak decline. Slopes are expressed in streamflow-percentile units per day. Complete daily observations over the respective windows were required.

(ii) **Relative precipitation timing.** We quantified precipitation timing relative to the streamflow peak as the mean relative day weighted by daily precipitation percentiles over a 15-day window centered on the annual maximum (Fig. 2). Days were indexed by $\tau$ from −7 to +7, with $\tau$ = 0 representing the streamflow peak day:

$$\bar{\tau}_P = \frac{\sum_{\tau=-7}^{7} \tau \cdot P_\tau}{\sum_{\tau=-7}^{7} P_\tau} \qquad (4)$$

$\bar{\tau}_P$ is the relative precipitation timing in days, $P_\tau$ is the daily precipitation percentile at relative day $\tau$. Negative values of $\bar{\tau}_P$ indicate precipitation concentrated before the streamflow peak, values near zero indicate precipitation centered near the peak day, and positive values indicate precipitation concentrated after the peak. Relative precipitation timing is generally expected to be non-positive, but can be positive when precipitation continues after the streamflow peak. We calculated it only foe windows with complete precipitation data and a positive sum of precipitation percentiles.

(iii) **Kernel-weighted temporal composites.** We constructed kernel-weighted composite profiles to examine temporal evolution of streamflow, precipitation, and soil moisture along the dominance gradient. For each event, daily percentile streamflow, precipitation, and soil moisture in the four layers were extracted over a 15-day window from $t - 7$ to $t + 7$, centered on the annual-maximum streamflow peak ($t$ = 0; Fig. 2). We ranked events by their *D*, and estimated composite profiles at the 10$^{th}$, 30$^{th}$, 50$^{th}$, 70$^{th}$, and 90$^{th}$ percentiles of its distribution. All retained events contributed to each profile with Gaussian weights determined by their percentile-rank distance from the target position:

https://doi.org/10.5194/egusphere-2026-6579
Preprint. Discussion started: 9 November 2026
© Author(s) 2026. CC BY 4.0 License.

$$w_i(q) = \exp\left[-\frac{1}{2}\left(\frac{r_i - q}{h}\right)^2\right] \qquad (5)$$

$w_i(q)$ is the weight assigned to event $i$ at target percentile rank $q$, $r_i$ is the percentile rank of event $i$ in the $D$ distribution, and $h = 0.10$ is the kernel bandwidth. For each variable and relative day, we calculated the composite value as the weighted mean across all available events. Events closer to the target position therefore received greater weight; more distant events contributed less. The $D$ value associated with each profile was the kernel-weighted mean $D$ of the contributing events.

The pre-peak diagnostic windows partly overlap the predictor windows, so associations with $D$ may partly reflect this overlap. These relationships describe characteristic event patterns and do not establish causal effects.

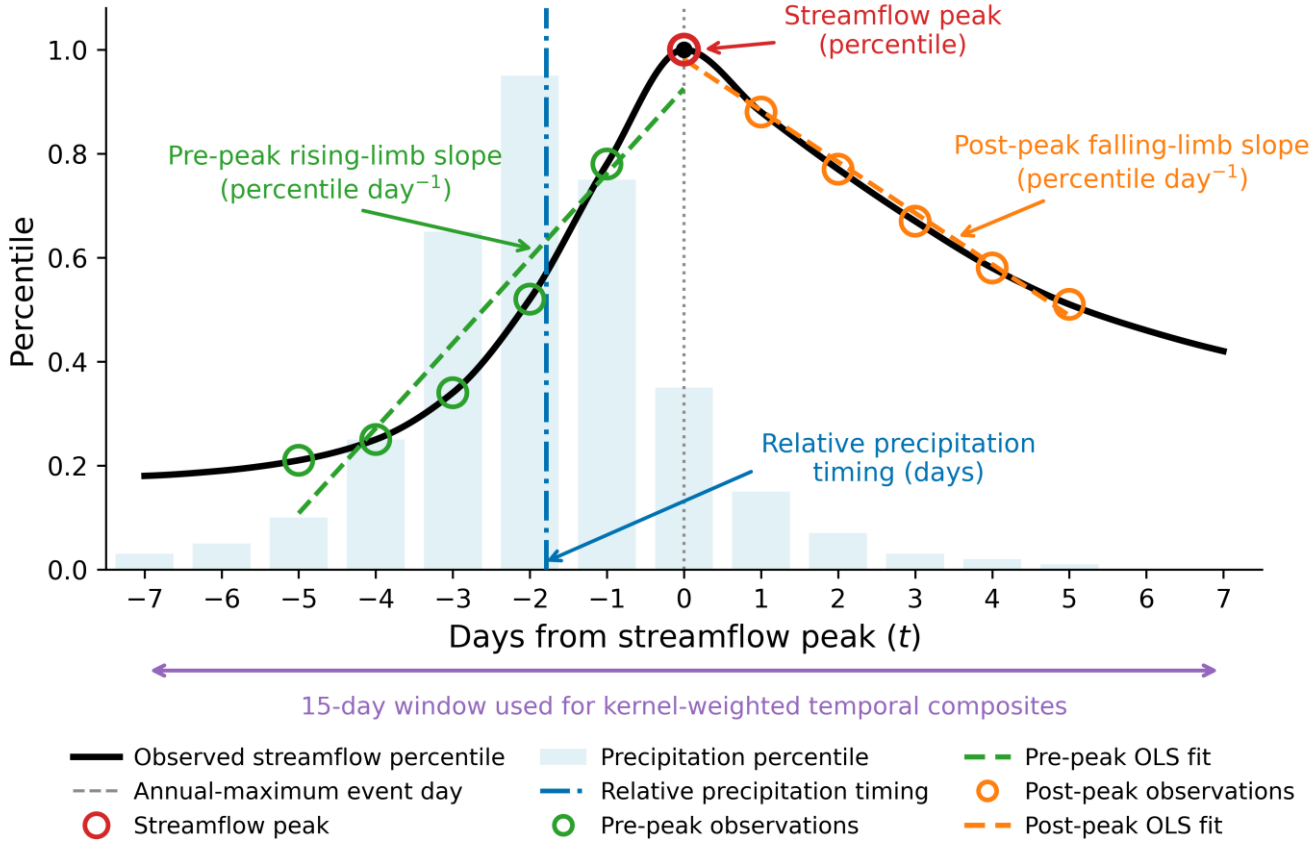



**Figure 2:** Schematic illustration of the event-scale hydrological diagnostics (Sect. 2.5.2). The annual-maximum event day is defined as $t$ = 0, and its observed streamflow percentile represents event magnitude (red circle). Near-peak hydrograph dynamics are quantified using ordinary least-squares (OLS) linear fits to all six observed daily streamflow-percentile values over $t - 5$ to $t$ for the pre-peak rising-limb slope (green) and $t$ to $t + 5$ for the post-peak falling-limb slope (orange). Circles mark observations and dashed lines the OLS fits; both fits include the red peak observation. The post-peak slope is multiplied by −1 so that larger positive values indicate a faster decline. Relative precipitation timing is the mean relative day weighted by daily precipitation percentiles over $t - 7$ to $t + 7$ (blue dash-dotted line); negative and positive values indicate precipitation concentrated before and after the streamflow peak, respectively. The same window is used to construct the kernel-weighted temporal composites of streamflow, precipitation, and soil moisture (purple arrow). The hydrograph and precipitation sequence are schematic.

https://doi.org/10.5194/egusphere-2026-6579
Preprint. Discussion started: 9 November 2026
© Author(s) 2026. CC BY 4.0 License.

### 2.5.3 Catchment-scale dominance

We aggregated event-level dominance indices within each catchment to characterize catchment-scale dominance patterns, and included only catchments with at least five retained annual-maximum events. We then defined catchment-scale dominance as the mean of event-level *D*:

$$\bar{D}_c = \frac{1}{n_c}\sum_{i=1}^{n_c} D_{i,c} \qquad (6)$$

$D_{i,c}$ is the dominance index of event *i* in catchment *c*, and $n_c$ is the number of retained events in that catchment. Thus, each annual-maximum event contributed equally to the catchment mean. Negative $\bar{D}_c$ values indicate stronger soil-moisture dominance on average across a catchment's annual-maximum events; positive values indicate stronger precipitation dominance. Values near zero indicate more balanced mean precipitation and soil-moisture contributions.

We then linked catchment-mean *D* to catchment area, elevation, terrain slope, water-table depth, clay fraction, aridity, and Köppen climate zone. The aridity index is the ratio of mean potential evapotranspiration to mean precipitation (PET/P), so larger values indicate greater aridity.

### 2.5.4 Statistical analysis

- **Event-scale relationships.** We quantified associations between *D* and streamflow percentile, near-peak hydrograph slopes, and relative precipitation timing using Spearman's rank correlation coefficient ($\rho$). Because catchments contributed multiple annual maxima, we assessed statistical significance using catchment-clustered inference to account for within-catchment dependence. *p*-values were adjusted together using the Benjamini–Hochberg false discovery rate (FDR) procedure. For visualization, we divided events into 20 approximately equal-count bins along *D*, and plotted each bin's median and interquartile range; correlations and significance tests used individual events rather than binned values.
- **Catchment attributes.** We assessed marginal associations between catchment-mean *D* and the six continuous catchment attributes using Spearman's $\rho$ across individual catchments, with FDR adjustment across the six marginal tests. For visualization, we divided catchments into 10 approximately equal-count bins of catchment-mean *D* and summarized each attribute's median and interquartile range per bin. Correlations and significance tests were based on individual catchments rather than the binned values. We examined attribute collinearity using pairwise Spearman correlations, and calculated partial correlations between catchment-mean *D* and each attribute while controlling for the other five. We rank-transformed all variables, removed control-attribute effects from both catchment-mean *D* and the focal attribute by linear regression, and correlated the residuals. Partial-correlation *p*-values were FDR-adjusted separately.
- **Climate-zone differences.** We evaluated differences in catchment-mean *D* among major Köppen climate zones using the Kruskal–Wallis test, reporting $\varepsilon^2$ as the effect size.

https://doi.org/10.5194/egusphere-2026-6579
Preprint. Discussion started: 9 November 2026
© Author(s) 2026. CC BY 4.0 License.

## 3 Results

### 3.1 Model predictive performance

The LightGBM model predicted streamflow percentile well across 1,374 catchments and approximately 17 million daily samples. All reported metrics used catchment-specific streamflow percentiles. Across the 25 validation-fold model fits, mean ± standard deviation performance was NSE = 0.575 ± 0.003, RMSE = 0.209 ± 0.001, and bias = 0.002 ± 0.002 percentile units, with little variation among fits. Catchment-wise NSE used the complete daily out-of-fold prediction series, averaging each day's five clipped out-of-fold predictions. Median catchment-wise NSE was 0.594 (Fig. 3a), with most catchments showing good predictive skill. For context, Kratzert et al. (2019b) reported median NSE values of 0.59–0.76 for a shared LSTM rainfall–runoff model across 531 catchments in the United States. Comparing our median catchment-wise NSE with Kratzert et al. (2019b) values is limited by differences in geographical scope, model structure, predictor set, and our target-percentile transformation. Nevertheless, the present model achieved a median NSE at the lower end of their reported range using only near-event precipitation and soil-moisture predictors. Across pooled daily out-of-fold predictions, 86.4 % of absolute errors were ≤ 0.3 percentile units (Fig. 3b); mean and median absolute errors were 0.157 and 0.121, respectively. These results support subsequent event-level interpretation, with SHAP analysis restricted to annual-maximum events satisfying the event-specific post-prediction quality controls in Sect. 2.4.

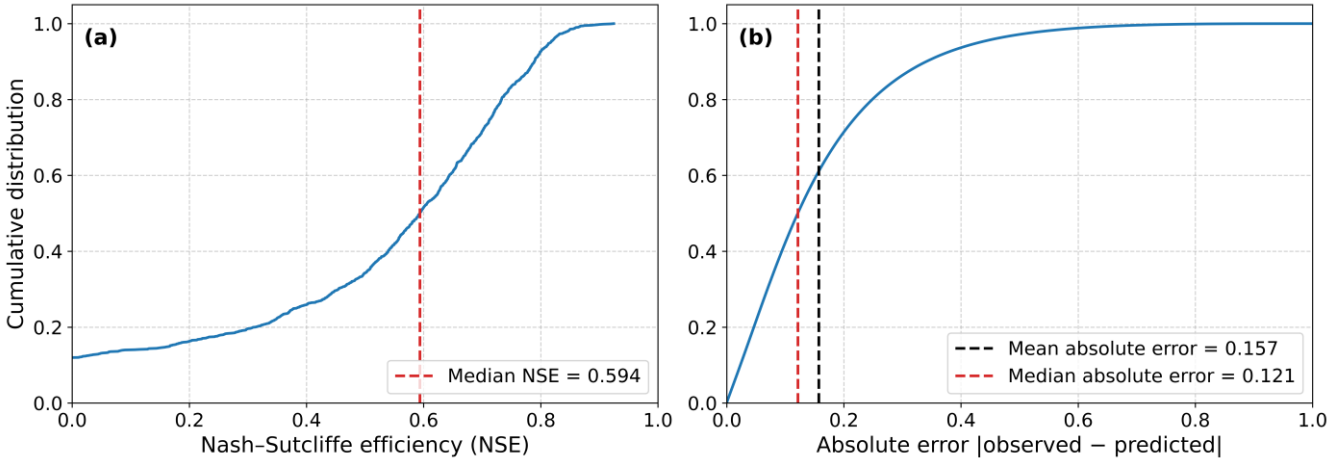



**Figure 3:** Model predictive performance. (a) Cumulative distribution of catchment-wise Nash–Sutcliffe efficiency (NSE) values calculated from the full validation series for 1,374 catchments. The red dashed line marks the median NSE of 0.594. The x-axis shows only NSE ≥ 0 to emphasize catchments with positive predictive skill; catchments with negative NSE are not displayed. (b) Cumulative distribution of absolute errors across approximately 17 million pooled out-of-fold daily predictions. The black and red dashed lines indicate the mean (0.157) and median (0.121) absolute error, respectively. SHAP-based interpretation retained only annual-maximum events with catchment NSE ≥ 0 and absolute prediction error ≤ 0.3 that also met the additional quality-control criteria in Sect. 2.4.

### 3.2 Precipitation–soil-moisture dominance in annual-maximum flood events

SHAP values quantified precipitation and antecedent soil-moisture contributions to each retained annual-maximum event's predicted streamflow percentile. In the SHAP summary plot (Fig. 4a), 3-day accumulated precipitation had the highest mean

https://doi.org/10.5194/egusphere-2026-6579
Preprint. Discussion started: 9 November 2026
© Author(s) 2026. CC BY 4.0 License.

absolute SHAP value, making it the most influential individual predictor overall. High precipitation and soil-moisture percentiles generally had positive SHAP values, contributing to higher predicted streamflow percentiles, whereas low predictor percentiles generally had negative SHAP values, contributing to lower predictions. Layer 3 (28–100 cm) had the highest mean absolute SHAP value among soil-moisture predictors and ranked second overall; layers 1, 2, and 4 contributed less.

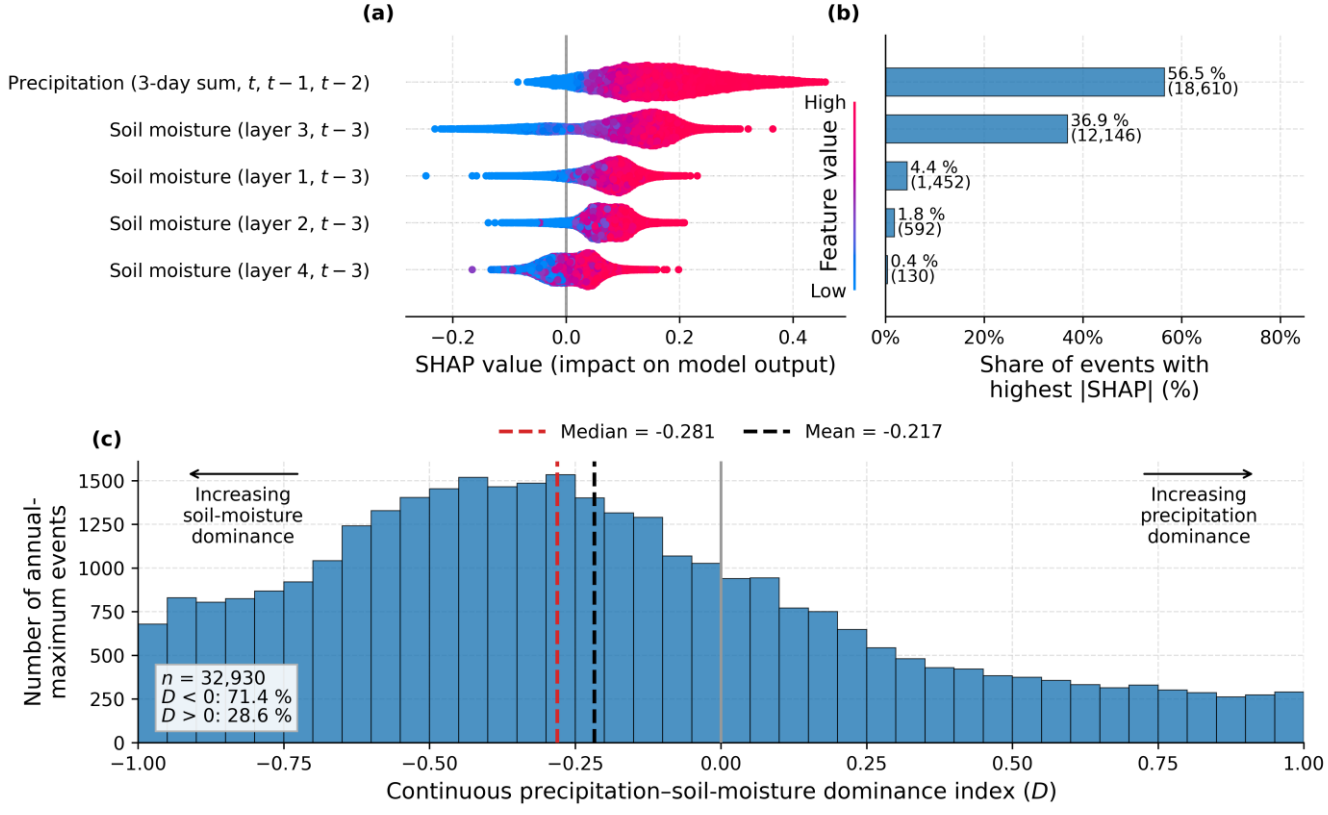



**Figure 4:** Predictor contributions and event-scale precipitation–soil-moisture dominance for 32,930 retained annual-maximum events. (a) SHAP summary plot, with predictors ordered by mean absolute SHAP value. Each point represents one event for a predictor; horizontal position shows its signed contribution to predicted streamflow percentile, and color shows its percentile from low (blue) to high (red). (b) Share of events in which each predictor had the largest absolute SHAP value. Labels report percentages and event counts. These frequencies concern individual predictors before combining the four soil-moisture layers' contributions. Soil-moisture layers 1–4 correspond to depths of 0–7, 7–28, 28–100, and 100–289 cm, respectively. (c) Distribution of the continuous precipitation–soil-moisture dominance index (*D*). Negative values indicate a net contribution magnitude across the four soil-moisture layers exceeding the absolute precipitation contribution; positive values indicate a larger precipitation contribution. The red and black dashed lines mark the median and mean, respectively; the gray vertical line marks $D = 0$.

The event-level ranking of individual predictors showed a similar pattern (Fig. 4b). Precipitation had the largest absolute SHAP value in 56.5 % of events, followed by soil moisture at layer 3 in 36.9 %. Layers 1, 2, and 4 were the strongest individual predictors in only 4.4 %, 1.8 %, and 0.4 % of events, respectively. These frequencies describe individual predictor prominence before combining the four soil-moisture layers' contributions.

Layer 3's prominence was sensitive to selected antecedent timing and does not establish that this depth alone physically controlled flood generation. The four soil-moisture predictors were strongly related, allowing SHAP to distribute shared

https://doi.org/10.5194/egusphere-2026-6579
Preprint. Discussion started: 9 November 2026
© Author(s) 2026. CC BY 4.0 License.

predictive information among layers in a model-dependent manner (Jiang et al., 2022b). In the sensitivity analysis, precipitation at $t - 1$ to $t$ with soil moisture at $t - 2$ increased layer 2's relative prominence, whereas the selected $t - 3$ soil-moisture configuration shifted prominence toward layer 3 (Supplement S2). Thus, the identified dominant depth partly depended on antecedent soil-moisture timing.

The continuous event-level dominance index $D$ (Eq. 2) compared the absolute precipitation contribution with the magnitude of the net contribution summed across the four soil-moisture layers (Fig. 4c). Across 32,930 retained annual-maximum events, $D$ had a mean of −0.217 and a median of −0.281, indicating an overall tendency toward soil-moisture dominance. In 71.4 % of events, the net soil-moisture contribution exceeded the precipitation contribution in magnitude ($D < 0$); in 28.6 %, the precipitation contribution was larger ($D > 0$). Thus, although precipitation was most frequently the strongest individual predictor, the grouped soil-moisture contribution was larger in most events.

Dominance varied substantially among events within individual catchments. Across the 1,154 catchments with at least 10 events, the median within-catchment standard deviation of $D$ was 0.404, while the standard deviation of catchment-mean $D$ was 0.244. For each event, we calculated the squared difference between its $D$ and its catchment mean, and between its catchment mean and the overall event mean. Summing these differences across events attributed 73.1 % of total variation to within-catchment differences and 26.9 % to between-catchment differences. Moreover, 94.2 % of catchments included both soil-moisture- and precipitation-dominated events, and 69.2 % had at least 20 % of events in each category. Thus, within-catchment event differences exceeded variation in catchment-mean dominance, supporting event-based analysis rather than treating dominance primarily as a fixed catchment characteristic.

### 3.3 Event-scale hydrological signatures of precipitation–soil-moisture dominance

The precipitation–antecedent wetness state space showed a continuous shift in event-scale dominance (Fig. 5a). As expected, $D$ generally increased with precipitation and decreased with antecedent profile wetness. High antecedent wetness maintained soil-moisture dominance across a broad range of precipitation conditions: even at high precipitation percentiles, $D$ often remained negative, although it shifted toward zero as precipitation increased. This pattern indicates a transition from predominantly soil-moisture control toward more balanced precipitation–soil-moisture contributions, rather than an abrupt switch between mechanisms. Mean annual-maximum streamflow percentile was high in two parts of the state space (Fig. 5b): moderate precipitation with very wet antecedent conditions, and very high precipitation with less elevated antecedent wetness. The largest streamflow percentiles occurred where precipitation and antecedent profile wetness were both high, associating the strongest floods with compounding rather than exclusively precipitation- or soil-moisture-dominated conditions.

The central event-scale question was whether flood magnitude, near-peak hydrograph dynamics, relative precipitation timing, and antecedent soil-moisture structure changed systematically from soil-moisture- to precipitation-dominated events.

Kernel-weighted composites complemented this analysis by showing streamflow, precipitation, and soil-moisture evolution around the annual-maximum streamflow peak along the dominance gradient (Fig. 6). All streamflow profiles rose to a sharp peak at $t = 0$, but pre-peak rises and post-peak recessions differed markedly with $D$ (Fig. 6a). Low-$D$ events began from

https://doi.org/10.5194/egusphere-2026-6579
Preprint. Discussion started: 9 November 2026
© Author(s) 2026. CC BY 4.0 License.

relatively elevated pre-event streamflow, rose gradually, and declined slowly after the peak. Their precipitation signal was broader and concentrated several days before the streamflow maximum (Fig. 6b). With increasing *D*, pre-peak streamflow was lower, the rise increasingly abrupt, and the post-peak decline steeper. Precipitation simultaneously became stronger and more concentrated immediately before the streamflow peak, with the highest-*D* profile peaking at approximately $t = -1$. Thus, precipitation-dominated events had precipitation concentrated closer to the streamflow peak, consistent with shorter precipitation-to-streamflow response times and sharper near-peak hydrographs.

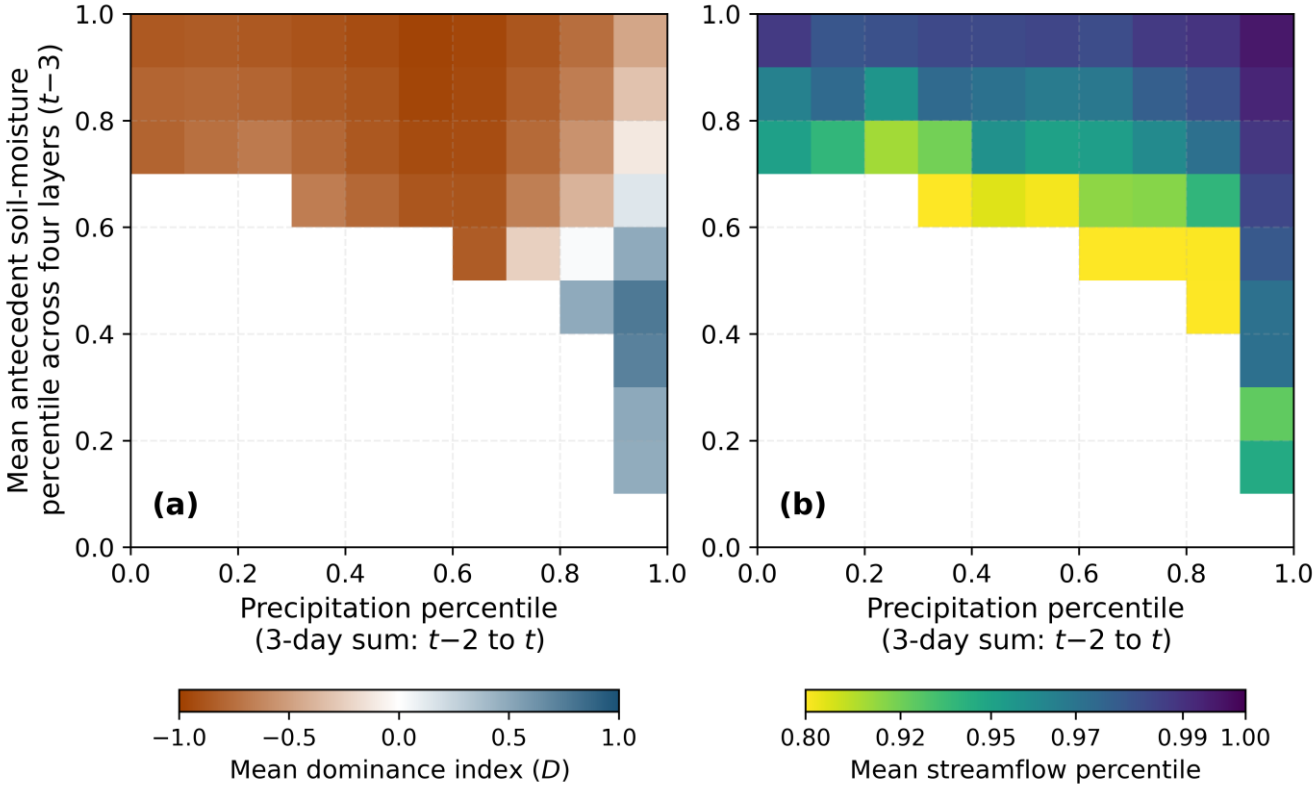



**Figure 5:** Joint variation in precipitation–soil-moisture dominance and annual-maximum streamflow percentile across the precipitation–antecedent wetness state space. (a) Cell colors show the mean continuous dominance index (*D*) per precipitation and soil-moisture bin; negative values indicate a larger grouped soil-moisture contribution and positive values a larger precipitation contribution. (b) Cell colors show the corresponding mean annual-maximum streamflow percentile, focusing on the high percentile range. Antecedent profile wetness is the mean of the four layer-specific soil-moisture percentiles at $t - 3$; precipitation is the percentile of the 3-day accumulation from $t - 2$ to $t$. Cells containing fewer than 10 events are not shown.

Peak streamflow percentiles differed only slightly between the 10$^{th}$- and 90$^{th}$-*D*-percentile profiles (0.977 and 0.982, respectively), as annual maxima occupy the upper tail of catchment-specific flow distributions. Corresponding kernel-weighted mean peak discharges were 9.49 and 23.68 mm d$^{-1}$. In a separate within-catchment comparison of 649 catchments with at least two events in both the bottom and top 20 % of the pooled D distribution, equally weighted catchment mean discharges were 9.35 and 15.82 mm d$^{-1}$, respectively.

https://doi.org/10.5194/egusphere-2026-6579
Preprint. Discussion started: 9 November 2026
© Author(s) 2026. CC BY 4.0 License.

Soil-moisture profiles showed simultaneous changes in antecedent wetness and vertical structure along the dominance gradient (Fig. 6c–f). At low *D*, pre-event soil moisture was already elevated throughout the profile. As *D* increased, antecedent soil moisture declined across all four layers, while near-peak responses became increasingly depth-dependent. In layers 1 and 2, high-*D* profiles rose rapidly just before the streamflow peak and largely converged with, or locally exceeded, low-*D* profiles near $t = 0$, consistent with rapid shallow-soil wetting during concentrated precipitation. In layers 3 and 4, dominance profiles remained separated throughout the event window: low-*D* events remained wetter than high-*D* events, which showed smaller near-peak increases in deep-layer soil moisture.

Together, the composites reveal a coherent transition in event timing and the vertical organization of antecedent wetness. Soil-moisture-dominated events combined elevated wetness throughout the soil profile with broader, earlier precipitation and more gradual hydrographs, whereas precipitation-dominated events combined drier antecedent conditions with concentrated pre-peak precipitation, rapid shallow-soil wetting, and sharper streamflow responses. Dominance profiles differed most in the days surrounding the streamflow peak, indicating a particular association between dominance and near-peak hydrograph behavior.

Spearman's $\rho$ quantified monotonic associations across individual events; medians within 20 equal-count bins of *D* illustrated each relationship's form (Fig. 7). Streamflow percentile showed a weak positive association with *D* ($\rho = 0.191$, FDR-adjusted $p$-value $< 0.001$; Fig. 7a), stronger within the soil-moisture-dominated range ($D < 0$; $\rho = 0.257$). The binned relationship was strongly nonlinear: median streamflow percentile rose sharply from its lowest values under strong soil-moisture dominance, then plateaued near the distribution's upper tail across balanced and precipitation-dominated conditions.

Near-peak hydrograph slopes changed more clearly across the dominance gradient. The 5-day pre-peak rising-limb slope showed the strongest association with *D* ($\rho = 0.466$, FDR-adjusted $p$-value $< 0.001$; Fig. 7b). Median rising-limb slopes increased progressively from approximately 0.02 percentile units per day at the lowest *D* values (soil-moisture dominance) to approximately 0.11 at the highest (precipitation dominance). This shift from slower pre-peak dynamics in soil-moisture-dominated events to faster rises in precipitation-dominated events agrees with the increasingly abrupt composite hydrograph rises (Fig. 6a). Because annual maxima occupy a narrow upper range of streamflow percentiles, fitted rising-limb slopes also reflect pre-peak flow levels, with higher initial percentiles leaving less scope for further increase toward the peak.

The 5-day post-peak falling-limb slope also increased with *D*, but less strongly ($\rho = 0.182$, FDR-adjusted $p$-value $< 0.001$; Fig. 7c). Median slopes increased from approximately 0.013 to 0.025 percentile units per day across the dominance gradient. The sign-reversed post-peak slope indicates faster decline at larger positive values. Thus, soil-moisture-dominated events receded more slowly, whereas precipitation-dominated events tended to recede faster, producing sharper near-peak hydrographs. This weaker association indicates that hydrographs differed most along the dominance gradient during the pre-peak rise.

Relative precipitation timing showed a weak positive association with *D* ($\rho = 0.156$, FDR-adjusted $p$-value $< 0.001$; Fig. 7d). Its median shifted from approximately −0.7 to −0.3 days between soil-moisture- and precipitation-dominated conditions. This shift toward zero indicates precipitation concentrated progressively nearer the streamflow peak, consistent with a shorter precipitation-to-streamflow response time as precipitation dominance increased. Recalculating this using precipitation depth (mm $d^{-1}$) rather than percentiles produced a slightly stronger association with *D* ($\rho = 0.228$; Supplement S4, Fig. S7).

https://doi.org/10.5194/egusphere-2026-6579
Preprint. Discussion started: 9 November 2026
© Author(s) 2026. CC BY 4.0 License.

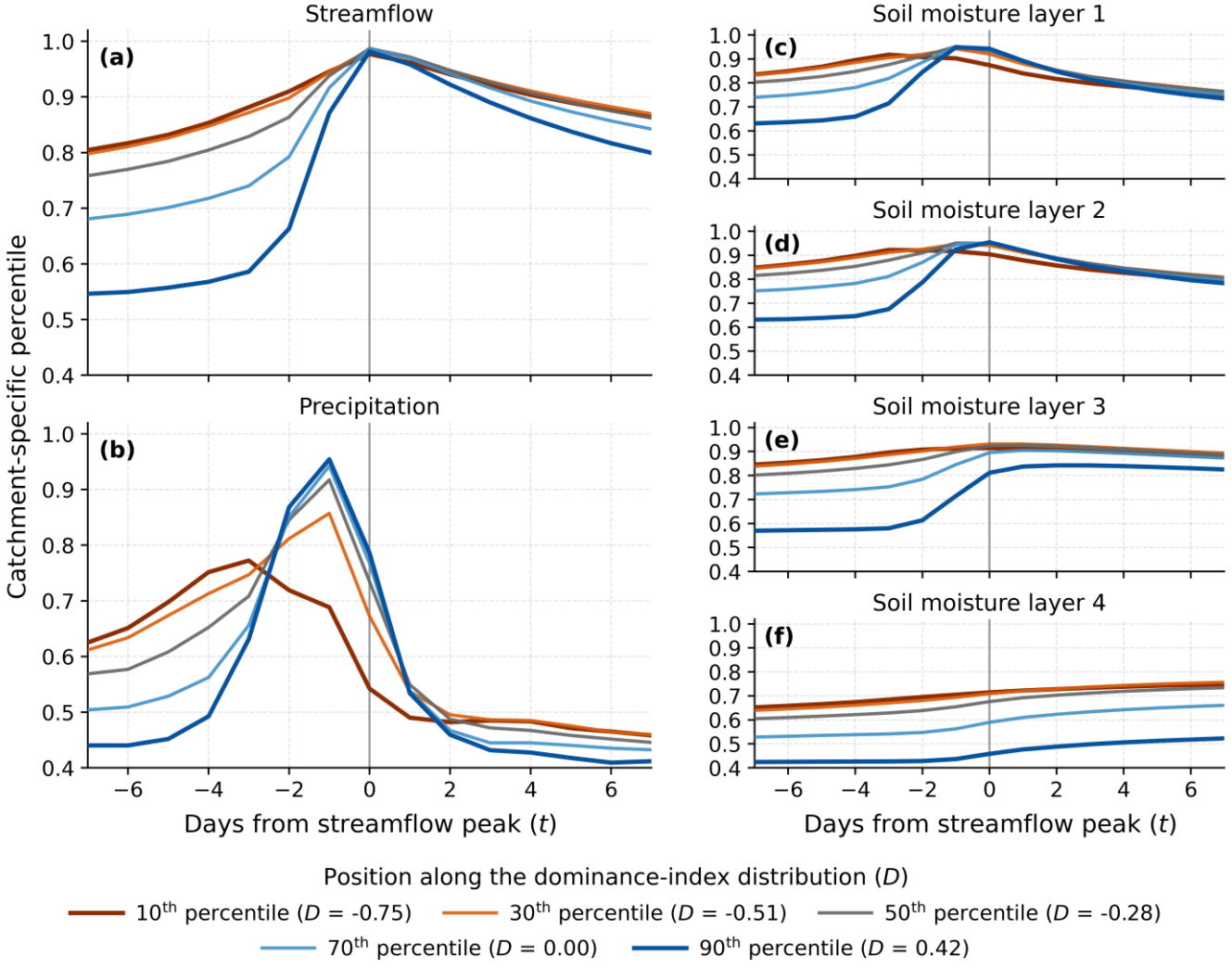



**Figure 6:** Kernel-weighted composite evolution of streamflow, precipitation, and soil moisture along the continuous dominance gradient. Panels show percentile profiles of (a) observed streamflow, (b) precipitation, and soil moisture in (c) layer 1 (0–7 cm), (d) layer 2 (7–28 cm), (e) layer 3 (28–100 cm), and (f) layer 4 (100–289 cm), from 7 days before to 7 days after the annual-maximum streamflow peak. Colored lines show kernel-weighted composites centered at the 10th, 30th, 50th, 70th, and 90th percentiles of the *D* distribution; legend values give each composite's kernel-weighted mean *D*. Each composite uses all retained events, weighting those closer to the target *D*-percentile rank more heavily. The gray vertical line marks the streamflow-peak day ($t = 0$).

Although event-scale associations differed markedly in magnitude, they showed a coherent transition from gradual flood dynamics with high antecedent wetness at low *D* to faster responses with concentrated near-peak precipitation at high *D*. Increasing precipitation dominance was most strongly associated with faster pre-peak streamflow rise and more weakly with faster post-peak recession, precipitation closer to the streamflow peak, and higher peak-flow percentile. Together with the soil-moisture composites, these patterns indicate that low-*D* floods develop from wetter antecedent conditions and evolve gradually, and high-*D* floods begin comparatively drier but respond faster to concentrated near-peak precipitation.

https://doi.org/10.5194/egusphere-2026-6579
Preprint. Discussion started: 9 November 2026
© Author(s) 2026. CC BY 4.0 License.

To assess whether Fig. 7 relationships reflected within-catchment event differences, we calculated catchment-specific Spearman correlations for 1,154 catchments with at least 10 events and pooled within-catchment correlations using catchment-demeaned ranks. For peak-streamflow percentile, rising-limb slope, falling-limb slope, and precipitation timing, median catchment-specific correlations were 0.082, 0.427, 0.114, and 0.161, and pooled within-catchment correlations were 0.092, 0.417, 0.127, and 0.157, respectively. Compared with Fig. 7, both analyses retained similar rising-limb slope and precipitation-timing associations but weaker peak-magnitude and recession associations. Thus, the observed relationships were not solely attributable to differences among catchments.

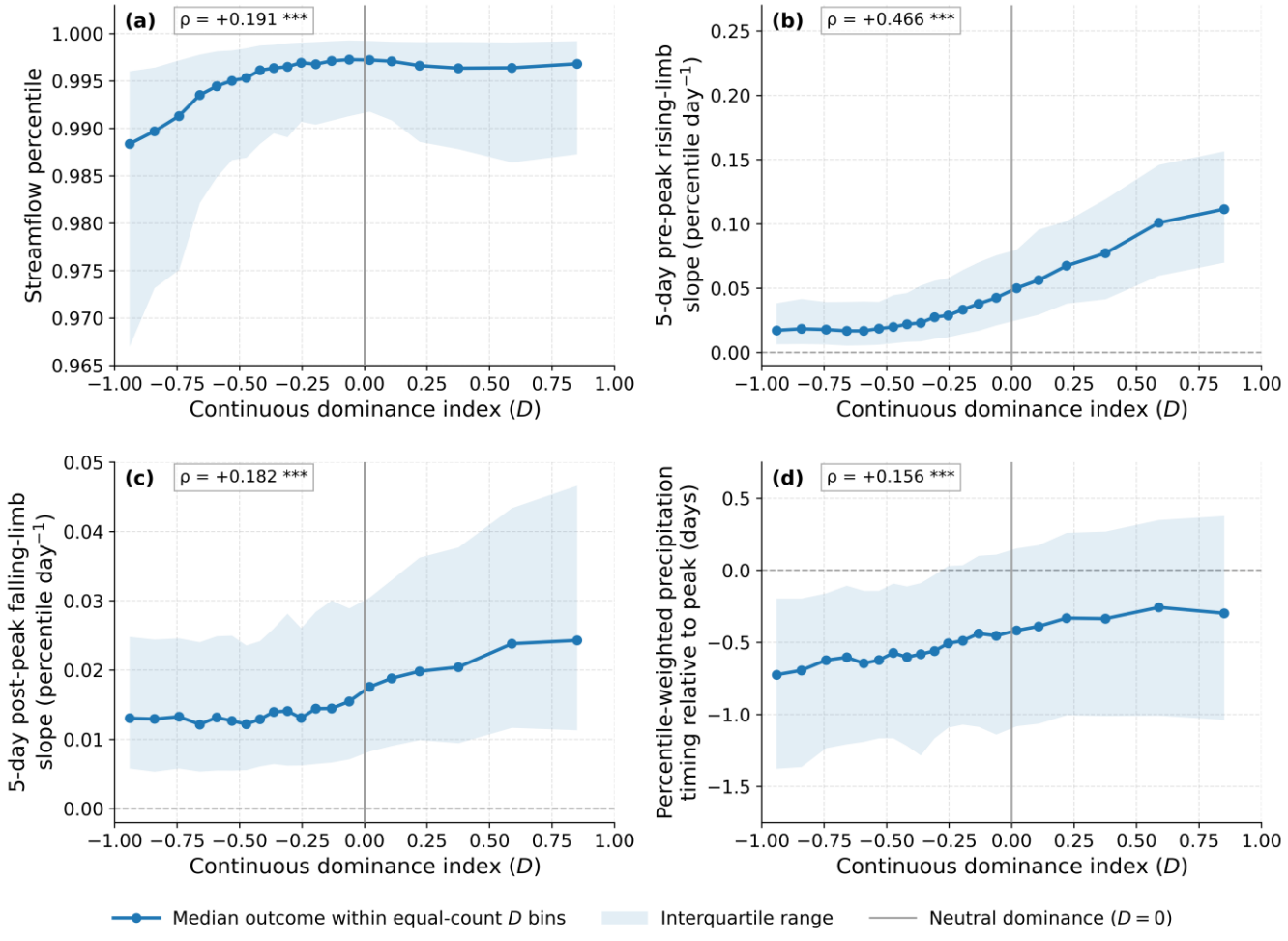



**Figure 7:** Event-scale hydrograph characteristics along the continuous precipitation–soil-moisture dominance gradient ($n$ = 32,930). Negative $D$ values indicate a larger soil-moisture contribution, and positive values indicate a larger precipitation contribution. For visualization, events were divided into 20 equal-count bins by $D$. Points and connecting lines show each bin's median outcome at its median $D$; shaded bands show the interquartile range. The gray vertical line marks $D = 0$, and horizontal dashed lines mark zero for the signed slope and precipitation-timing metrics. Panels show (a) annual-maximum streamflow percentile, (b) 5-day pre-peak rising-limb slope, (c) 5-day post-peak falling-limb slope, and (d) relative precipitation timing. Annotations report Spearman's rank correlation coefficient $\rho$ across individual events and FDR-adjusted significance represented by asterisks: $*$ $p$-value < 0.05, $**$ $p$-value < 0.01, and $***$ $p$-value < 0.001; n.s. indicates $p$-value ≥ 0.05.

https://doi.org/10.5194/egusphere-2026-6579
Preprint. Discussion started: 9 November 2026
© Author(s) 2026. CC BY 4.0 License.

### 3.4 Associations between catchment characteristics and precipitation–soil-moisture dominance

Catchment-scale dominance was the mean event-level $D$ for 1,199 catchments (out of 1,209) with at least five retained annual-maximum events. The distribution was shifted toward negative values, with a mean of −0.204 and a median of −0.179 (Fig. 8). Overall, 80.2 % of catchments had mean $D < 0$, indicating average soil-moisture dominance across annual-maximum events, whereas 19.8 % had mean $D > 0$, indicating average precipitation dominance.

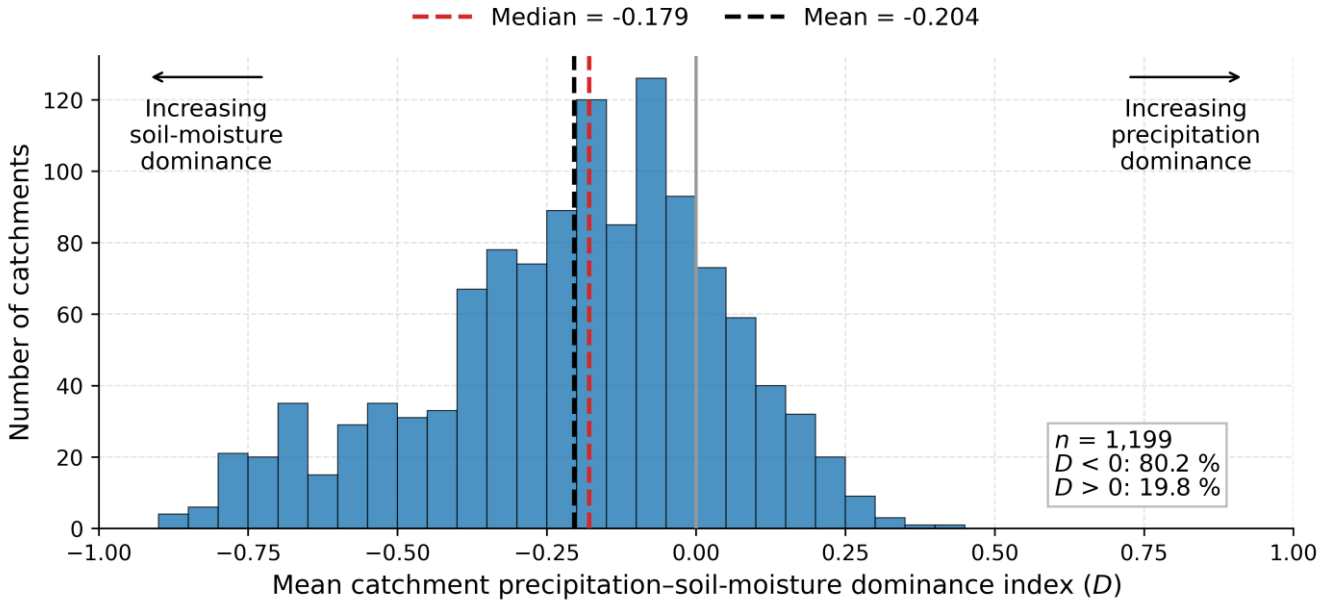



**Figure 8:** Distribution of mean catchment-scale precipitation–soil-moisture dominance. Histogram of mean event-level dominance index ($D$) for 1,199 catchments with at least five retained annual-maximum events. Negative values indicate soil-moisture-dominated catchments and positive values indicate precipitation-dominated catchments. The gray vertical line marks $D = 0$; red and black dashed lines mark the median (−0.179) and mean (−0.204), respectively. Overall, 80.2 % of catchments had mean $D < 0$, and 19.8 % had mean $D > 0$.

Catchment attributes showed contrasting marginal associations with mean $D$ (Fig. 9). Catchment area decreased with increasing $D$ ($\rho = -0.284$; Fig. 9a), whereas elevation ($\rho = 0.273$; Fig. 9b), terrain slope ($\rho = 0.517$; Fig. 9c), and water-table depth ($\rho = 0.457$; Fig. 9d) increased (all FDR-adjusted $p$-values < 0.001). Marginal associations with clay fraction and aridity were very small ($\rho = 0.045$ and 0.068; Fig. 9e and 9f, respectively). However, several attributes were strongly correlated, particularly terrain slope with water-table depth ($\rho = 0.765$), elevation with water-table depth ($\rho = 0.702$), and elevation with terrain slope ($\rho = 0.594$; Supplement S4, Fig. S8). After controlling for the other five attributes, terrain slope retained the largest association with mean $D$ (partial $\rho = 0.286$), followed by catchment area (−0.185; both FDR-adjusted $p$-values < 0.001). The remaining partial correlations were small ($|\rho| \leq 0.085$). Thus, smaller and steeper catchments tended toward greater precipitation dominance after adjustment; weaker elevation and water-table-depth associations suggest that their marginal patterns largely reflected variation shared with other attributes.

https://doi.org/10.5194/egusphere-2026-6579
Preprint. Discussion started: 9 November 2026
© Author(s) 2026. CC BY 4.0 License.

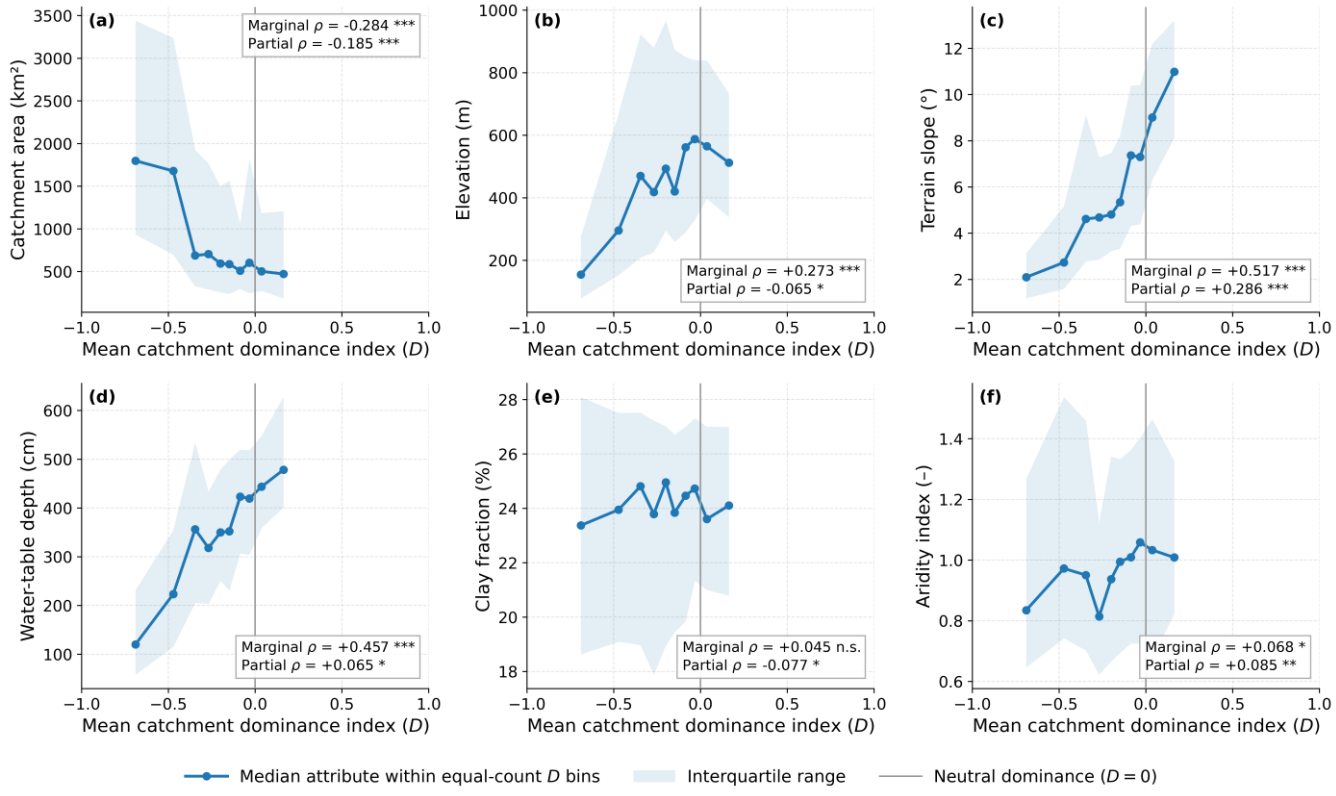



**Figure 9:** Catchment attributes along the continuous dominance gradient. Relationships between mean catchment dominance index (*D*) and (a) catchment area, (b) elevation, (c) terrain slope, (d) water-table depth, (e) clay fraction, and (f) aridity index for 1,199 catchments with at least five retained annual-maximum events. Catchments were divided into 10 approximately equal-count bins by mean *D*; points and lines show each bin's median attribute value, and shaded bands its interquartile range. These lines and bands represent the marginal binned relationships. The gray vertical line marks $D = 0$. Annotations report marginal Spearman correlations and partial Spearman correlations controlling for the other five attributes. Correlations used individual catchments rather than binned values; marginal and partial *p*-values were separately FDR-adjusted across the six attributes. Asterisks indicate $*$ *p*-value < 0.05, $**$ *p*-value < 0.01, and $***$ *p*-value < 0.001; n.s. indicates *p*-value ≥ 0.05.

Mean catchment *D* also differed among the major Köppen climate zones (Kruskal–Wallis $\varepsilon^2 = 0.091$, *p*-value < 0.001; Fig. 10). Median *D* was negative in all four zones, consistent with the catchment distribution's overall shift toward soil-moisture dominance (Fig. 8). Tropical catchments showed the strongest soil-moisture dominance, with a median *D* of −0.42, compared with −0.12 in dry, −0.15 in temperate, and −0.19 in continental catchments. The tropical distribution was clearly shifted toward negative *D*, whereas the dry, temperate, and continental distributions overlapped substantially. Dry catchments had the median closest to zero and thus the greatest average tendency toward precipitation dominance among the four zones, consistent with aridity's weak positive association with *D* (Fig. 9f). Climate-zone differences therefore appear primarily to reflect tropical catchments' markedly stronger soil-moisture dominance. However, broad, overlapping within-zone distributions indicate substantial within-zone catchment variation; patterns for the dry and continental zones warrant caution because of their smaller sample sizes.

https://doi.org/10.5194/egusphere-2026-6579
Preprint. Discussion started: 9 November 2026
© Author(s) 2026. CC BY 4.0 License.

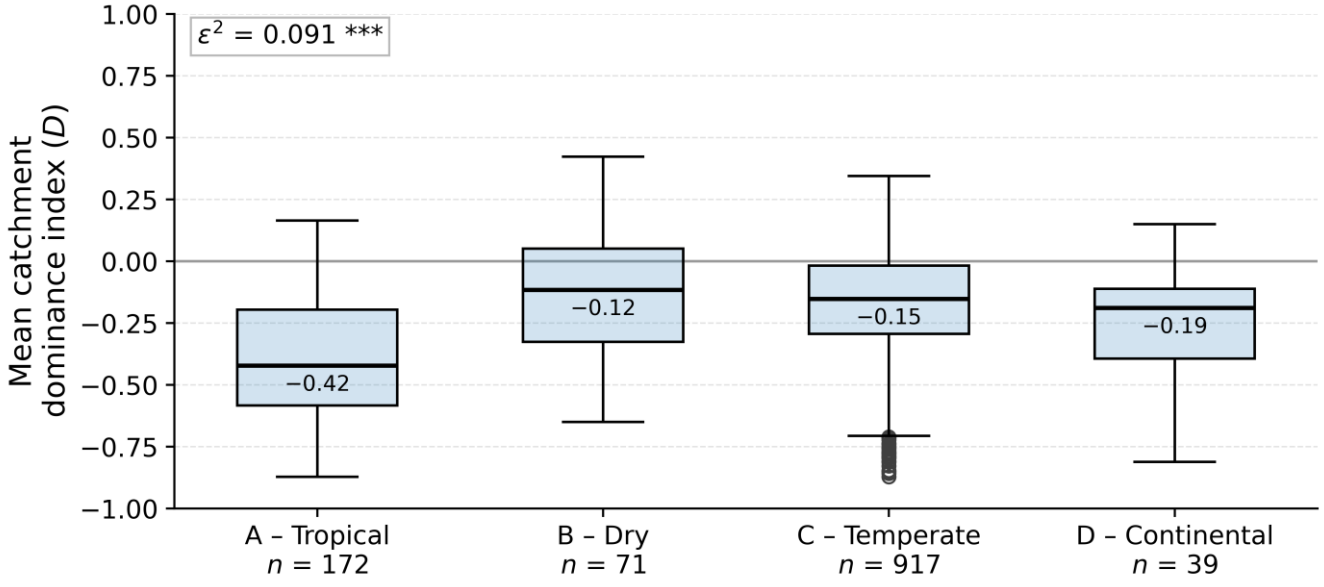



**Figure 10:** Mean catchment precipitation–soil-moisture dominance across major Köppen climate zones. Boxplots show the distribution of mean catchment dominance index (*D*) for tropical ($n$ = 172), dry ($n$ = 71), temperate ($n$ = 917), and continental ($n$ = 39) catchments. Negative values indicate more soil-moisture-dominated floods, and positive values indicate more precipitation-dominated floods. Boxes show the interquartile range, horizontal lines indicate medians, and whiskers extend to the most extreme observations within 1.5 times the interquartile range of the lower and upper quartiles; points beyond the whiskers are shown as outliers. The gray horizontal line marks $D = 0$. The annotation gives the Kruskal–Wallis effect size ($\varepsilon^2 = 0.091$); *** indicates overall climate-zone differences at $p$-value < 0.001.

## 4 Discussion

### 4.1 Precipitation–soil-moisture dominance and flood-generation dynamics

The results support viewing flood generation as a continuous balance between event forcing and antecedent catchment state rather than fixed flood types. The framework's main advance is quantifying this balance continuously for individual floods within a catchment-shared model using relative predictive contributions of near-event precipitation and multi-depth antecedent soil moisture, and linking it directly to flood behavior. This differs from approaches assigning events to discrete mechanisms or summarizing controls primarily at catchment level. These approaches provide valuable process classifications; our continuous event-level framework additionally resolves dominance gradations, within-catchment variability, and their links to flood behavior. The results reveal two high-flow pathways: moderate precipitation on very wet antecedent conditions, and very large precipitation inputs on comparatively drier conditions. Similar flood magnitudes can therefore emerge from different combinations of forcing and antecedent wetness, consistent with previous work emphasizing their joint control on flood generation (e.g., Brunner and Dougherty, 2022; Ivancic and Shaw, 2015; Stein et al., 2020; Wasko and Nathan, 2019).

The dominance balance was clearly expressed in rising-limb development. Soil-moisture-dominated events were associated with wetter antecedent conditions and evolved more gradually, whereas precipitation-dominated events showed lower pre-event streamflow, precipitation concentrated closer to the flood peak, and substantially faster pre-peak rises. Post-peak decline

https://doi.org/10.5194/egusphere-2026-6579
Preprint. Discussion started: 9 November 2026
© Author(s) 2026. CC BY 4.0 License.

also accelerated with increasing precipitation dominance, but the relationship was much weaker than for the rising limb. Thus, the precipitation–soil-moisture balance might be expressed more clearly in flood development than recession. This asymmetry is hydrologically plausible because event forcing and antecedent state influence the rising phase more immediately, whereas recession integrates broader storage and drainage controls (Mathai and Mujumdar, 2022). The dominance gradient therefore captures a transition from slower responses associated with high antecedent wetness to sharper, more precipitation-linked flood dynamics.

The soil-moisture composites add a vertical dimension to this interpretation. At high *D*, precipitation influence appeared primarily as rapid shallow-soil wetting; at low *D*, elevated antecedent wetness extended throughout the soil profile, indicating that deeper soil-moisture conditions also contributed to flood generation. This contrast between rapid shallow wetting and persistent deeper-layer differences is consistent with studies showing that multi-layer soil moisture improves modeled root-zone dynamics (He et al., 2025) and that shallow and intermediate soil depths can play distinct roles in hydrological connectivity and runoff generation (Singh et al., 2021). Individual layer rankings nevertheless warrant caution because soil-moisture predictors are correlated and their relative SHAP contributions depend partly on antecedent timing. Thus, the robust signal is the vertical contrast itself rather than the apparent dominance of any single soil layer.

The event-based perspective shows that dominance is not fixed within individual catchments. Within-catchment event variation exceeded between-catchment variation, and within-catchment associations showed that event-scale relationships were not solely attributable to catchment composition. Most catchments also contained floods on both sides of the continuum, consistent with evidence of coexisting flood-generating mechanisms within catchments (e.g., Cui and Tian, 2026; Jiang et al., 2022b; Stein et al., 2020). Our framework extends this perspective by retaining the relative strength of precipitation and soil-moisture contributions as a continuous quantity rather than assigning each flood a single mechanism class. It also complements multi-driver approaches, as recent rainfall and antecedent soil moisture commonly act together in flood generation (Jiang et al., 2024a). Thus, *D* preserves the controls' relative balance and its event-to-event variability.

At catchment scale, greater precipitation dominance was associated with smaller and steeper catchments, even after adjustment for the other attributes. This agrees with regional findings by Ran et al. (2022) and large-sample evidence by Stein et al. (2021) and Jiang et al. (2022b) linking catchment size and slope to flood-dominant controls and generating processes. Our results extend these relationships using continuous event-level precipitation–soil-moisture contributions. However, adjustment substantially attenuated positive marginal associations with elevation and water-table depth, suggesting that they largely reflected variation shared with the other attributes. The weak aridity association and overlapping dominance across climate zones may suggest that physiographic characteristics differentiated dominance more clearly than broad hydroclimatic setting. Beyond identifying whether precipitation or soil moisture contributes more to predictions, the framework links their event-to-event balance to flood magnitude, hydrograph dynamics, the vertical structure of antecedent wetness, and catchment setting.

https://doi.org/10.5194/egusphere-2026-6579
Preprint. Discussion started: 9 November 2026
© Author(s) 2026. CC BY 4.0 License.

### 4.2 Potential implications of climate change for precipitation–soil-moisture dominance patterns

This study characterizes historical event-level precipitation–soil-moisture dominance but does not assess temporal trends in response to climate change. Nevertheless, distinguishing precipitation- and soil-moisture-dominated floods offers a perspective on potential shifts in flood-generating controls. Climate change can modify precipitation forcing and antecedent wetness differently, altering their relative influence on flood generation (Blöschl et al., 2017, 2019). Previous studies show that decreasing soil moisture can offset increasing rainfall for more moderate floods, whereas increasingly extreme precipitation can dominate larger events (Bertola et al., 2021; Brunner et al., 2021; Rinat et al., 2026; Wasko and Nathan, 2019). Globally, flood-magnitude and duration changes were more strongly associated with antecedent wetness, and frequency changes with heavy rainfall, though both drivers influenced all three flood dimensions (Liu et al., 2022).

Temporal changes in flood-generating controls further support this perspective. Jiang et al. (2022a) identified temporal shifts among flood-generating mechanisms across Europe. Tarasova et al. (2023) showed that transitions between rainfall on dry and wet soils contributed strongly to regional flood anomalies. Xu et al. (2024) detected dominant flood-driver changes in more than 40 % of 482 US catchments. Continental-scale observations linked European flood-timing shifts to changes in snowmelt, extreme-precipitation timing, and soil-moisture maxima (Blöschl et al., 2017), and regional flood-magnitude trends to different combinations of rainfall, soil moisture, evaporation, and snowmelt (Blöschl et al., 2019). These findings suggest that flood non-stationarity may involve shifts in the relative influence of event forcing and antecedent states, rather than precipitation alone.

The continuous *D* framework could support future analyses of such shifts. Conceptually, under drier antecedent conditions, larger storage deficits may partly absorb moderate precipitation increases, whereas sufficient extreme precipitation can overcome these deficits and increase precipitation dominance. Conversely, wetter antecedent states could strengthen soil-moisture influence by allowing high flows under moderate precipitation. Changes in the vertical soil-moisture distribution may further modify this balance by altering shallow-soil wetting and deeper antecedent storage. Because higher *D* was associated with faster pre-peak rises and precipitation concentrated closer to the streamflow peak, temporal dominance shifts could accompany changes in hydrograph dynamics. We did not test whether *D* has changed over time. Applying this framework temporally could therefore test whether flood-generation controls are shifting and whether these shifts change flood behavior.

### 4.3 Large-sample, machine-learning-driven importance analysis

The framework combines event-level contribution analysis with large-sample, catchment-shared modeling. Joint learning across diverse catchments broadens the training envelope compared to catchment-specific models and promotes more generalizable relationships (Addor et al., 2020; Kratzert et al., 2024; Slater et al., 2025). *D*'s consistency with hydrograph dynamics, relative precipitation timing, vertical soil-moisture evolution, and catchment characteristics supports the hydrological relevance of model-derived contribution patterns.

https://doi.org/10.5194/egusphere-2026-6579
Preprint. Discussion started: 9 November 2026
© Author(s) 2026. CC BY 4.0 License.

SHAP contributions should nevertheless be interpreted as predictive rather than causal. They describe how the fitted model uses precipitation and soil moisture to predict streamflow and may reflect model structure, predictor dependence, data uncertainty, and temporal representation (Jiang et al., 2024b; Slater et al., 2025). This is particularly relevant for correlated soil-moisture layers, whose shared predictive information may be distributed among depths (Jiang et al., 2024b). Grouping contributions reduces reliance on potentially unstable layer-specific importance, but *D* remains an index of relative model-attributed precipitation and soil-moisture influence rather than a causal partition of flood-generation processes.

Several design choices strengthen this interpretation. SHAP analysis used only held-out, well-predicted annual maxima from catchments with positive predictive skill, as meaningful model interpretation requires reliable predictions (Murdoch et al., 2019; Xu et al., 2024). Repeated two-level cross-validation reduced information leakage, while restricting predictors maintained explicit interpretability of the two targeted controls. With independent hydrological diagnostics, these safeguards reduce the risk of interpreting poorly represented events or model artifacts. The framework shows how interpretable machine learning can complement process-based hydrology by identifying nonlinear, event-specific patterns across diverse catchments while retaining cross-catchment comparability.

### 4.4 Limitations and future work

Several limitations shape the study scope. While ERA5-Land provides consistent multi-continental precipitation and multi-depth soil moisture, reanalysis uncertainties remain, and daily catchment-averaged data cannot resolve sub-daily storm structure or spatial heterogeneity. Consequently, short-lived precipitation forcing may be underrepresented, especially in small or arid catchments, potentially biasing the analysis toward slowly varying controls such as soil moisture. Higher-resolution observations or alternative datasets could further test these event-scale patterns. Additionally, because ERA5-Land simulates soil moisture using precipitation forcing from the same framework, these variables are not fully independent (Muñoz-Sabater et al., 2021). This shared origin may introduce related uncertainties to consider when interpreting the relative model-attributed contributions of precipitation and soil moisture.

Soil-moisture depths require cautious interpretation because ERA5-Land's fixed layers may not match actual soil depth in every catchment. In shallow-soil settings, such as arid or highly eroded catchments, deeper modeled layers may therefore correspond poorly to hydrologically active soil storage. Grouping the four soil-moisture SHAP contributions permits comparison of their combined influence with precipitation, but opposing layer contributions can partly offset one another. Moreover, the relative prominence of individual layers changed under alternative antecedent timings. Layer rankings should not be interpreted as identifying a unique physical depth controlling runoff; broader vertical contrasts persisting across temporal composites and sensitivity analyses warrant greater confidence.

The percentile transformation enabled direct cross-catchment comparison of different hydroclimatic regimes within a catchment-shared model but removed information on absolute magnitude: identical precipitation or streamflow percentiles can represent substantially different physical values among catchments (Sect. 3.3). Catchment-shared training broadened the represented hydroclimatic conditions and can support generalization and improve predictions of extremes (Frame et al., 2022;

https://doi.org/10.5194/egusphere-2026-6579
Preprint. Discussion started: 9 November 2026
© Author(s) 2026. CC BY 4.0 License.

Kratzert et al., 2024; Nearing et al., 2024), but predictive performance based on historical sample cannot be assumed to extend to unprecedented hydrological extremes beyond this training envelope. Clipping individual out-of-fold predicted percentiles to [0, 1] before averaging mapped out-of-range values to the corresponding boundary, removing their degree of exceedance. As an event-level diagnostic, averaging the five raw out-of-fold predictions yielded values outside [0, 1] for 88 of 32,930 retained annual-maximum events (0.267 %), all above 1 (maximum = 1.060); none were below 0 (minimum = 0.323). Although rare, clipping prevents differentiation beyond the percentile bounds. Future applications could avoid truncation using a target representation without fixed percentile bounds. The framework thus characterizes relative hydrological states and dynamics within its historical domain, rather than unprecedented extremes or universally transferable precipitation and discharge thresholds.

The spatial domain also constrains generalization, as some climate settings were underrepresented and snow-influenced catchments were intentionally excluded to avoid additional process complexity. Extending to these regions would require snowpack, temperature, and melt-related predictors, along with reservoirs, land cover, and human influences, where relevant. Finally, this study evaluates spatial and event-to-event differences in $D$, rather than temporal changes. Future analyses using higher-resolution or projected hydroclimatic data could test whether the precipitation–soil-moisture balance changes over time and whether these shifts accompany changes in flood dynamics.

## 5 Conclusions

This study developed a multi-continental, event-based framework combining a catchment-shared LightGBM model with SHAP to quantify the relative predictive contributions of near-event precipitation and multi-depth antecedent soil moisture to annual-maximum floods. The continuous dominance index ($D$) preserves variation among individual floods rather than assigning them to fixed process classes; it expresses model-attributed predictive contributions rather than a causal partition of flood-generating processes. The main findings are:

- **Similar flood magnitudes arose from markedly different combinations of forcing and antecedent storage**. High flows occurred both under moderate precipitation over very wet soils and under very high precipitation over comparatively drier conditions, the latter with increasing precipitation dominance. Although 3-day precipitation was the strongest individual predictor in 56.5 % of the 32,930 annual maxima, the grouped net soil-moisture contribution exceeded it in 71.4 % (66.6–87.8 % across the tested predictor configurations).
- **The dominance balance was expressed more clearly in flood development than in magnitude or recession**. Increasing $D$ was associated most strongly with faster pre-peak rises ($\rho$ = 0.466), and weakly with higher peaks, faster post-peak recession, and precipitation concentrated closer to the streamflow peak ($\rho$ = 0.156–0.191). The rising-limb association persisted within catchments ($\rho$ = 0.417). Soil-moisture-dominated floods developed from wetter profiles and evolved gradually, whereas precipitation-dominated floods began drier and showed rapid shallow-layer wetting with sharper streamflow responses, while deeper layers remained drier throughout the event window.

https://doi.org/10.5194/egusphere-2026-6579
Preprint. Discussion started: 9 November 2026
© Author(s) 2026. CC BY 4.0 License.

- **Catchment properties shaped average dominance, but dominance was not a fixed catchment property**. Greater precipitation dominance remained associated with steeper (partial $\rho = 0.286$) and smaller (partial $\rho = -0.185$) catchments, whereas climate zones differentiated dominance less clearly. Within-catchment differences nevertheless accounted for 73.1 % of the total variation in $D$, and 94.2 % of catchments with at least 10 events contained both soil-moisture- and precipitation-dominated floods.

Overall, flood behavior cannot be read from precipitation or antecedent wetness alone, but from their event-specific balance. Quantifying that balance continuously, and linking it to hydrograph dynamics, the vertical structure of antecedent wetness, and catchment setting, provides a consistent basis for comparing flood-generation controls across events and catchments.

## Code and data availability

The code used in this analysis will be provided in a GitHub repository (to be added after review). The GRDC-Caravan extension dataset is publicly available on Zenodo: https://doi.org/10.5281/zenodo.15349031 (Färber et al., 2025b).

## Supplement link

The link to the supplement will be included by Copernicus, if applicable.

## Author contributions

YK and EM conceptualized the work and developed the methodology. YK performed data analysis, visualization, manuscript writing, review, and editing. EM provided supervision, funding acquisition, manuscript review, and editing.

## Competing interests

The authors declare that they have no conflict of interest.

## Disclaimer

Copernicus Publications remains neutral with regard to jurisdictional claims made in the text, published maps, institutional affiliations, or any other geographical representation in this paper. While Copernicus Publications makes every effort to include appropriate place names, the final responsibility lies with the authors. Views expressed in the text are those of the authors and do not necessarily reflect the views of the publisher.

https://doi.org/10.5194/egusphere-2026-6579
Preprint. Discussion started: 9 November 2026
© Author(s) 2026. CC BY 4.0 License.

**Acknowledgements**

During the preparation of this work, the authors used ChatGPT and Gemini to assist with code generation and copy-editing of the manuscript. These tools were not used to generate scientific claims, equations, or parameter values; all such content is traceable to the authors' own analyses or cited literature. After using these tools, the authors reviewed and edited all AI-assisted text to ensure consistency with the methods and results presented, and take full responsibility for the content of the published article.

**Financial support**

This study was supported by the Israel Science Foundation (ISF) grant no. 1999/22, the Ministry of Environmental Protection research scholarship for environmental research, the Women's League of Israel research scholarship for environmental research, and the Hebrew University excellence scholarship.

**Review statement**

The review statement will be added by Copernicus Publications listing the handling editor as well as all contributing referees according to their status anonymous or identified.

**References**

Addor, N., Do, H. X., Alvarez-Garreton, C., Coxon, G., Fowler, K., and Mendoza, P. A.: Large-sample hydrology: recent progress, guidelines for new datasets and grand challenges, Hydrol. Sci. J., 65, 712–725, https://doi.org/10.1080/02626667.2019.1683182, 2020.

Bandhauer, M., Isotta, F., Lakatos, M., Lussana, C., Båserud, L., Izsák, B., Szentes, O., Tveito, O. E., and Frei, C.: Evaluation of daily precipitation analyses in E-OBS (v19.0e) and ERA5 by comparison to regional high-resolution datasets in European regions, Int. J. Climatol., 42, 727–747, https://doi.org/10.1002/joc.7269, 2022.

Beck, H. E., Pan, M., Roy, T., Weedon, G. P., Pappenberger, F., van Dijk, A. I. J. M., Huffman, G. J., Adler, R. F., and Wood, E. F.: Daily evaluation of 26 precipitation datasets using Stage-IV gauge-radar data for the CONUS, Hydrol. Earth Syst. Sci., 23, 207–224, https://doi.org/10.5194/hess-23-207-2019, 2019.

Beck, H. E., Pan, M., Miralles, D. G., Reichle, R. H., Dorigo, W. A., Hahn, S., Sheffield, J., Karthikeyan, L., Balsamo, G., Parinussa, R. M., van Dijk, A. I. J. M., Du, J., Kimball, J. S., Vergopolan, N., and Wood, E. F.: Evaluation of 18 satellite- and model-based soil moisture products using in situ measurements from 826 sensors, Hydrol. Earth Syst. Sci., 25, 17–40, https://doi.org/10.5194/HESS-25-17-2021, 2021.

https://doi.org/10.5194/egusphere-2026-6579
Preprint. Discussion started: 9 November 2026
© Author(s) 2026. CC BY 4.0 License.

Berghuijs, W. R., Woods, R. A., Hutton, C. J., and Sivapalan, M.: Dominant flood generating mechanisms across the United States, Geophys. Res. Lett., 43, 4382–4390, https://doi.org/10.1002/2016GL068070, 2016.

Berghuijs, W. R., Harrigan, S., Molnar, P., Slater, L. J., and Kirchner, J. W.: The Relative Importance of Different Flood-Generating Mechanisms Across Europe, Water Resour. Res., 55, 4582–4593, https://doi.org/10.1029/2019WR024841, 2019.

Bertola, M., Viglione, A., Vorogushyn, S., Lun, D., Merz, B., and Blöschl, G.: Do small and large floods have the same drivers of change? A regional attribution analysis in Europe, Hydrol. Earth Syst. Sci., 25, 1347–1364, https://doi.org/10.5194/HESS-25-1347-2021, 2021.

Blöschl, G., Hall, J., Parajka, J., Perdigão, R. A. P., Merz, B., Arheimer, B., Aronica, G. T., Bilibashi, A., Bonacci, O., Borga, M., Čanjevac, I., Castellarin, A., Chirico, G. B., Claps, P., Fiala, K., Frolova, N., Gorbachova, L., Gül, A., Hannaford, J., Harrigan, S., Kireeva, M., Kiss, A., Kjeldsen, T. R., Kohnová, S., Koskela, J. J., Ledvinka, O., Macdonald, N., Mavrova-Guirguinova, M., Mediero, L., Merz, R., Molnar, P., Montanari, A., Murphy, C., Osuch, M., Ovcharuk, V., Radevski, I., Rogger, M., Salinas, J. L., Sauquet, E., Šraj, M., Szolgay, J., Viglione, A., Volpi, E., Wilson, D., Zaimi, K., and Živković, N.: Changing climate shifts timing of European floods, Science, 357, 588–590, https://doi.org/10.1126/science.aan2506, 2017.

Blöschl, G., Hall, J., Viglione, A., Perdigão, R. A. P., Parajka, J., Merz, B., Lun, D., Arheimer, B., Aronica, G. T., Bilibashi, A., Boháč, M., Bonacci, O., Borga, M., Čanjevac, I., Castellarin, A., Chirico, G. B., Claps, P., Frolova, N., Ganora, D., Gorbachova, L., Gül, A., Hannaford, J., Harrigan, S., Kireeva, M., Kiss, A., Kjeldsen, T. R., Kohnová, S., Koskela, J. J., Ledvinka, O., Macdonald, N., Mavrova-Guirguinova, M., Mediero, L., Merz, R., Molnar, P., Montanari, A., Murphy, C., Osuch, M., Ovcharuk, V., Radevski, I., Salinas, J. L., Sauquet, E., Šraj, M., Szolgay, J., Volpi, E., Wilson, D., Zaimi, K., and Živković, N.: Changing climate both increases and decreases European river floods, Nature, 573, 108–111, https://doi.org/10.1038/s41586-019-1495-6, 2019.

Brunner, M. I. and Dougherty, E. M.: Varying Importance of Storm Types and Antecedent Conditions for Local and Regional Floods, Water Resour. Res., 58, e2022WR033249, https://doi.org/10.1029/2022WR033249, 2022.

Brunner, M. I., Slater, L., Tallaksen, L. M., and Clark, M.: Challenges in modeling and predicting floods and droughts: A review, WIREs Water, 8, e1520, https://doi.org/10.1002/wat2.1520, 2021.

Collins, M. J.: River flood seasonality in the Northeast United States: Characterization and trends, Hydrol. Process., 33, 687–698, https://doi.org/10.1002/HYP.13355, 2019.

Cui, Z. and Tian, F.: Runoff thresholds, runoff generation mechanisms, and catchment characteristics: a global synthesis, Hydrol. Earth Syst. Sci., 30, 5281–5296, https://doi.org/10.5194/HESS-30-5281-2026, 2026.

Dorigo, W., van Oevelen, P., Wagner, W., Drusch, M., Mecklenburg, S., Robock, A., and Jackson, T.: A New International Network for in Situ Soil Moisture Data, Eos Trans. AGU, 92, 141–142, https://doi.org/10.1029/2011EO170001, 2011.

Dorigo, W., Himmelbauer, I., Aberer, D., Schremmer, L., Petrakovic, I., Zappa, L., Preimesberger, W., Xaver, A., Annor, F., Ardö, J., Baldocchi, D., Bitelli, M., Blöschl, G., Bogena, H., Brocca, L., Calvet, J.-C., Camarero, J. J., Capello, G., Choi, M., Cosh, M. C., van de Giesen, N., Hajdu, I., Ikonen, J., Jensen, K. H., Kanniah, K. D., de Kat, I., Kirchengast, G., Kumar Rai, P., Kyrouac, J., Larson, K., Liu, S., Loew, A., Moghaddam, M., Martínez Fernández, J., Mattar Bader, C., Morbidelli, R.,

https://doi.org/10.5194/egusphere-2026-6579
Preprint. Discussion started: 9 November 2026
© Author(s) 2026. CC BY 4.0 License.

Musial, J. P., Osenga, E., Palecki, M. A., Pellarin, T., Petropoulos, G. P., Pfeil, I., Powers, J., Robock, A., Rüdiger, C., Rummel, U., Strobel, M., Su, Z., Sullivan, R., Tagesson, T., Varlagin, A., Vreugdenhil, M., Walker, J., Wen, J., Wenger, F., Wigneron, J. P., Woods, M., Yang, K., Zeng, Y., Zhang, X., Zreda, M., Dietrich, S., Gruber, A., van Oevelen, P., Wagner, W., Scipal, K., Drusch, M., and Sabia, R.: The International Soil Moisture Network: serving Earth system science for over a decade, Hydrol. Earth Syst. Sci., 25, 5749–5804, https://doi.org/10.5194/hess-25-5749-2021, 2021.

Färber, C., Plessow, H., Mischel, S. A., Kratzert, F., Addor, N., Shalev, G., and Looser, U.: GRDC-Caravan: extending Caravan with data from the Global Runoff Data Centre, Earth Syst. Sci. Data, 17, 4613–4625, https://doi.org/10.5194/ESSD-17-4613-2025, 2025a.

Färber, C., Plessow, H., Mischel, S., Kratzert, F., Addor, N., Shalev, G., and Looser, U.: GRDC-Caravan: extending the original dataset with data from the Global Runoff Data Centre, version 0.6, Zenodo [data set], https://doi.org/10.5281/zenodo.15349031, 2025b.

Frame, J. M., Kratzert, F., Klotz, D., Gauch, M., Shalev, G., Gilon, O., Qualls, L. M., Gupta, H. V., and Nearing, G. S.: Deep learning rainfall–runoff predictions of extreme events, Hydrol. Earth Syst. Sci., 26, 3377–3392, https://doi.org/10.5194/hess-26-3377-2022, 2022.

He, Y., Mao, H., Wang, C., Hu, J., Ninsawat, S., Song, X., Jing, G., Li, R., Wang, M., and Duan, Z.: Advancing hydrological modeling through multivariate calibration of multi-layer soil moisture dynamics, J. Hydrol. Reg. Stud., 57, 102125, https://doi.org/10.1016/j.ejrh.2024.102125, 2025.

Hersbach, H., Bell, B., Berrisford, P., Hirahara, S., Horányi, A., Muñoz-Sabater, J., Nicolas, J., Peubey, C., Radu, R., Schepers, D., Simmons, A., Soci, C., Abdalla, S., Abellan, X., Balsamo, G., Bechtold, P., Biavati, G., Bidlot, J., Bonavita, M., De Chiara, G., Dahlgren, P., Dee, D., Diamantakis, M., Dragani, R., Flemming, J., Forbes, R., Fuentes, M., Geer, A., Haimberger, L., Healy, S., Hogan, R. J., Hólm, E., Janisková, M., Keeley, S., Laloyaux, P., Lopez, P., Lupu, C., Radnoti, G., de Rosnay, P., Rozum, I., Vamborg, F., Villaume, S., and Thépaut, J.-N.: The ERA5 global reanalysis, Q. J. R. Meteorol. Soc., 146, 1999–2049, https://doi.org/10.1002/qj.3803, 2020.

Ivancic, T. J. and Shaw, S. B.: Examining why trends in very heavy precipitation should not be mistaken for trends in very high river discharge, Clim. Change, 133, 681–693, https://doi.org/10.1007/s10584-015-1476-1, 2015.

Jiang, Q., Li, W., Fan, Z., He, X., Sun, W., Chen, S., Wen, J., Gao, J., and Wang, J.: Evaluation of the ERA5 reanalysis precipitation dataset over Chinese Mainland, J. Hydrol., 595, 125660, https://doi.org/10.1016/j.jhydrol.2020.125660, 2021.

Jiang, S., Bevacqua, E., and Zscheischler, J.: River flooding mechanisms and their changes in Europe revealed by explainable machine learning, Hydrol. Earth Syst. Sci., 26, 6339–6359, https://doi.org/10.5194/hess-26-6339-2022, 2022a.

Jiang, S., Zheng, Y., Wang, C., and Babovic, V.: Uncovering Flooding Mechanisms Across the Contiguous United States Through Interpretive Deep Learning on Representative Catchments, Water Resour. Res., 58, e2021WR030185, https://doi.org/10.1029/2021WR030185, 2022b.

Jiang, S., Tarasova, L., Yu, G., and Zscheischler, J.: Compounding effects in flood drivers challenge estimates of extreme river floods, Sci. Adv., 10, eadl4005, https://doi.org/10.1126/sciadv.adl4005, 2024a.

https://doi.org/10.5194/egusphere-2026-6579
Preprint. Discussion started: 9 November 2026
© Author(s) 2026. CC BY 4.0 License.

Jiang, S., Sweet, L., Blougouras, G., Brenning, A., Li, W., Reichstein, M., Denzler, J., Shangguan, W., Yu, G., Huang, F., and Zscheischler, J.: How Interpretable Machine Learning Can Benefit Process Understanding in the Geosciences, Earth's Future, 12, e2024EF004540, https://doi.org/10.1029/2024EF004540, 2024b.

Ke, G., Meng, Q., Finley, T., Wang, T., Chen, W., Ma, W., Ye, Q., and Liu, T.-Y.: LightGBM: A Highly Efficient Gradient Boosting Decision Tree, in: Proceedings of the 31st International Conference on Neural Information Processing Systems, Long Beach, CA, USA, 4–9 December 2017, 3149–3157, https://proceedings.neurips.cc/paper_files/paper/2017/hash/6449f44a102fde848669bdd9eb6b76fa-Abstract.html, 2017.

Knoben, W. J. M., Woods, R. A., and Freer, J. E.: A Quantitative Hydrological Climate Classification Evaluated With Independent Streamflow Data, Water Resour. Res., 54, 5088–5109, https://doi.org/10.1029/2018WR022913, 2018.

Kratzert, F., Klotz, D., Brenner, C., Schulz, K., and Herrnegger, M.: Rainfall–runoff modelling using Long Short-Term Memory (LSTM) networks, Hydrol. Earth Syst. Sci., 22, 6005–6022, https://doi.org/10.5194/hess-22-6005-2018, 2018.

Kratzert, F., Klotz, D., Herrnegger, M., Sampson, A. K., Hochreiter, S., and Nearing, G. S.: Toward Improved Predictions in Ungauged Basins: Exploiting the Power of Machine Learning, Water Resour. Res., 55, 11344–11354, https://doi.org/10.1029/2019WR026065, 2019a.

Kratzert, F., Klotz, D., Shalev, G., Klambauer, G., Hochreiter, S., and Nearing, G.: Towards learning universal, regional, and local hydrological behaviors via machine learning applied to large-sample datasets, Hydrol. Earth Syst. Sci., 23, 5089–5110, https://doi.org/10.5194/hess-23-5089-2019, 2019b.

Kratzert, F., Nearing, G., Addor, N., Erickson, T., Gauch, M., Gilon, O., Gudmundsson, L., Hassidim, A., Klotz, D., Nevo, S., Shalev, G., and Matias, Y.: Caravan - A global community dataset for large-sample hydrology, Sci. Data, 10, 61, https://doi.org/10.1038/s41597-023-01975-w, 2023.

Kratzert, F., Gauch, M., Klotz, D., and Nearing, G.: HESS Opinions: Never train a Long Short-Term Memory (LSTM) network on a single basin, Hydrol. Earth Syst. Sci., 28, 4187–4201, https://doi.org/10.5194/HESS-28-4187-2024, 2024.

Linke, S., Lehner, B., Ouellet Dallaire, C., Ariwi, J., Grill, G., Anand, M., Beames, P., Burchard-Levine, V., Maxwell, S., Moidu, H., Tan, F., and Thieme, M.: Global hydro-environmental sub-basin and river reach characteristics at high spatial resolution, Sci. Data, 6, 283, https://doi.org/10.1038/s41597-019-0300-6, 2019.

Liu, J., Feng, S., Gu, X., Zhang, Y., Beck, H. E., Zhang, J., and Yan, S.: Global changes in floods and their drivers, J. Hydrol., 614, 128553, https://doi.org/10.1016/J.JHYDROL.2022.128553, 2022.

Lundberg, S. M. and Lee, S.-I.: A unified approach to interpreting model predictions, in: Proceedings of the 31st International Conference on Neural Information Processing Systems, Long Beach, CA, USA, 4–9 December 2017, 4768–4777, https://papers.nips.cc/paper_files/paper/2017/hash/8a20a8621978632d76c43dfd28b67767-Abstract.html, 2017.

Lundberg, S. M., Erion, G., Chen, H., DeGrave, A., Prutkin, J. M., Nair, B., Katz, R., Himmelfarb, J., Bansal, N., and Lee, S.-I.: From local explanations to global understanding with explainable AI for trees, Nat. Mach. Intell., 2, 56–67, https://doi.org/10.1038/s42256-019-0138-9, 2020.

https://doi.org/10.5194/egusphere-2026-6579
Preprint. Discussion started: 9 November 2026
© Author(s) 2026. CC BY 4.0 License.

Mathai, J. and Mujumdar, P. P.: Use of streamflow indices to identify the catchment drivers of hydrographs, Hydrol. Earth Syst. Sci., 26, 2019–2033, https://doi.org/10.5194/hess-26-2019-2022, 2022.

Merz, R. and Blöschl, G.: A process typology of regional floods, Water Resour. Res., 39, 1340, https://doi.org/10.1029/2002WR001952, 2003.

Muñoz-Sabater, J., Dutra, E., Agustí-Panareda, A., Albergel, C., Arduini, G., Balsamo, G., Boussetta, S., Choulga, M., Harrigan, S., Hersbach, H., Martens, B., Miralles, D. G., Piles, M., Rodríguez-Fernández, N. J., Zsoter, E., Buontempo, C., and Thépaut, J.-N.: ERA5-Land: a state-of-the-art global reanalysis dataset for land applications, Earth Syst. Sci. Data, 13, 4349–4383, https://doi.org/10.5194/essd-13-4349-2021, 2021.

Murdoch, W. J., Singh, C., Kumbier, K., Abbasi-Asl, R., and Yu, B.: Definitions, methods, and applications in interpretable machine learning, Proc. Natl. Acad. Sci. U. S. A., 116, 22071–22080, https://doi.org/10.1073/PNAS.1900654116, 2019.

Nearing, G., Cohen, D., Dube, V., Gauch, M., Gilon, O., Harrigan, S., Hassidim, A., Klotz, D., Kratzert, F., Metzger, A., Nevo, S., Pappenberger, F., Prudhomme, C., Shalev, G., Shenzis, S., Tekalign, T. Y., Weitzner, D., and Matias, Y.: Global prediction of extreme floods in ungauged watersheds, Nature, 627, 559–563, https://doi.org/10.1038/s41586-024-07145-1, 2024.

Ran, Q., Wang, J., Chen, X., Liu, L., Li, J., and Ye, S.: The relative importance of antecedent soil moisture and precipitation in flood generation in the middle and lower Yangtze River basin, Hydrol. Earth Syst. Sci., 26, 4919–4931, https://doi.org/10.5194/HESS-26-4919-2022, 2022.

Rinat, Y., Armon, M., and Morin, E.: The complex effect of climate change and urbanization on streamflow in small–medium eastern Mediterranean catchments, Hydrol. Earth Syst. Sci., 30, 4565–4585, https://doi.org/10.5194/HESS-30-4565-2026, 2026.

Shapley, L. S.: 17. A Value for n-Person Games, in: Contributions to the Theory of Games (AM-28), Volume II, edited by: Kuhn, H. W. and Tucker, A. W., Princeton University Press, 307–318, https://doi.org/10.1515/9781400881970-018, 1953.

Sharma, A., Wasko, C., and Lettenmaier, D. P.: If Precipitation Extremes Are Increasing, Why Aren't Floods?, Water Resour. Res., 54, 8545–8551, https://doi.org/10.1029/2018WR023749, 2018.

Shen, C.: A Transdisciplinary Review of Deep Learning Research and Its Relevance for Water Resources Scientists, Water Resour. Res., 54, 8558–8593, https://doi.org/10.1029/2018WR022643, 2018.

Shen, M. and Chui, T. F. M.: Quantifying the relative contributions of different flood generating mechanisms to floods across CONUS, J. Hydrol., 626, 130255, https://doi.org/10.1016/J.JHYDROL.2023.130255, 2023.

Singh, N. K., Emanuel, R. E., McGlynn, B. L., and Miniat, C. F.: Soil Moisture Responses to Rainfall: Implications for Runoff Generation, Water Resour. Res., 57, e2020WR028827, https://doi.org/10.1029/2020WR028827, 2021.

Slater, L., Blougouras, G., Deng, L., Deng, Q., Ford, E., Hoek van Dijke, A., Huang, F., Jiang, S., Liu, Y., Moulds, S., Schepen, A., Yin, J., and Zhang, B.: Challenges and opportunities of ML and explainable AI in large-sample hydrology, Philos. Trans. R. Soc. A, 383, 20240287, https://doi.org/10.1098/RSTA.2024.0287, 2025.

Stein, L., Pianosi, F., and Woods, R.: Event-based classification for global study of river flood generating processes, Hydrol. Process., 34, 1514–1529, https://doi.org/10.1002/hyp.13678, 2020.

https://doi.org/10.5194/egusphere-2026-6579
Preprint. Discussion started: 9 November 2026
© Author(s) 2026. CC BY 4.0 License.

Stein, L., Clark, M. P., Knoben, W. J. M., Pianosi, F., and Woods, R. A.: How Do Climate and Catchment Attributes Influence Flood Generating Processes? A Large-Sample Study for 671 Catchments Across the Contiguous USA, Water Resour. Res., 57, e2020WR028300, https://doi.org/10.1029/2020WR028300, 2021.

Su, J., Wang, X., Ren, W., and Liu, W.: Decomposing precipitation biases into frequency and intensity components: Comparative analysis of IMERG and ERA5-Land over the Tibetan Plateau, Atmos. Res., 326, 108320, https://doi.org/10.1016/J.ATMOSRES.2025.108320, 2025.

Tang, G., Clark, M. P., Papalexiou, S. M., Ma, Z., and Hong, Y.: Have satellite precipitation products improved over last two decades? A comprehensive comparison of GPM IMERG with nine satellite and reanalysis datasets, Remote Sens. Environ., 240, 111697, https://doi.org/10.1016/J.RSE.2020.111697, 2020.

Tarasova, L., Merz, R., Kiss, A., Basso, S., Blöschl, G., Merz, B., Viglione, A., Plötner, S., Guse, B., Schumann, A., Fischer, S., Ahrens, B., Anwar, F., Bárdossy, A., Bühler, P., Haberlandt, U., Kreibich, H., Krug, A., Lun, D., Müller-Thomy, H., Pidoto, R., Primo, C., Seidel, J., Vorogushyn, S., and Wietzke, L.: Causative classification of river flood events, WIREs Water, 6, e1353, https://doi.org/10.1002/WAT2.1353, 2019.

Tarasova, L., Basso, S., and Merz, R.: Transformation of Generation Processes From Small Runoff Events to Large Floods, Geophys. Res. Lett., 47, e2020GL090547, https://doi.org/10.1029/2020GL090547, 2020.

Tarasova, L., Lun, D., Merz, R., Blöschl, G., Basso, S., Bertola, M., Miniussi, A., Rakovec, O., Samaniego, L., Thober, S., and Kumar, R.: Shifts in flood generation processes exacerbate regional flood anomalies in Europe, Commun. Earth Environ., 4, 49, https://doi.org/10.1038/s43247-023-00714-8, 2023.

Wasko, C. and Nathan, R.: Influence of changes in rainfall and soil moisture on trends in flooding, J. Hydrol., 575, 432–441, https://doi.org/10.1016/j.jhydrol.2019.05.054, 2019.

Wasko, C., Nathan, R., Stein, L., and O'Shea, D.: Evidence of shorter more extreme rainfalls and increased flood variability under climate change, J. Hydrol., 603, 126994, https://doi.org/10.1016/J.JHYDROL.2021.126994, 2021.

Xu, J., Ma, Z., Yan, S., and Peng, J.: Do ERA5 and ERA5-land precipitation estimates outperform satellite-based precipitation products? A comprehensive comparison between state-of-the-art model-based and satellite-based precipitation products over mainland China, J. Hydrol., 605, 127353, https://doi.org/10.1016/J.JHYDROL.2021.127353, 2022.

Xu, Y., Lin, K., Hu, C., Chen, X., Zhang, J., Xiao, M., and Xu, C. Y.: Uncovering the Dynamic Drivers of Floods Through Interpretable Deep Learning, Earth's Future, 12, e2024EF004751, https://doi.org/10.1029/2024EF004751, 2024.